Dual-Readout Calorimetry for High-Quality Energy Measurements

Proposal and request for beam time

to CERN's SPS Committee

by the DREAM Collaboration

(Cagliari – Cosenza – Iowa State – Pavia – Pisa – Roma I – Texas Tech)

CERN-SPSC-2010-012 / SPSC-M-771
31/03/2010

Presented by:

Dr. Richard Wigmans[1]

Texas Tech University

April 13, 2010

[1]Spokesperson. Tel. [806] 742 3779, FAX [806] 742 1182, E-mail: wigmans@ttu.edu

Membership of the DREAM Collaboration

N. Akchurin[a], A. Basti[b], F. Bedeschi[b], A. Cardini[c], G. Ciapetti[d], R. Ferrari[e], S. Franchino[f], M. Fraternali[f], G. Gaudio[e], J. Hauptman[g], M. Incagli[b], F. Lacava[d], L. La Rotonda[h], S. Lee[g], M. Livan[f], E. Meoni[h,1], A. Negri[f], D. Pinci[d], A. Policicchio[h,2], S. Popescu[a], F. Scuri[b], A. Sill[a], G. Susinno[h], W. Vandelli[i], T. Venturelli[h], C. Voena[d], I. Volobouev[a] and R. Wigmans[a]

[a] *Texas Tech University, Lubbock (TX), USA*
[b] *Dipartimento di Fisica, Università di Pisa and INFN Sezione di Pisa, Italy*
[c] *Dipartimento di Fisica, Università di Cagliari and INFN Sezione di Cagliari, Italy*
[d] *Dipartimento di Fisica, Università di Roma "La Sapienza" and INFN Sezione di Roma, Italy*
[e] *INFN Sezione di Pavia, Italy*
[f] *INFN Sezione di Pavia and Dipartimento di Fisica Nucleare e Teorica, Università di Pavia, Italy*
[g] *Iowa State University, Ames (IA), USA*
[h] *Dipartimento di Fisica, Università della Calabria and INFN Cosenza, Italy*
[i] *CERN, Genève, Switzerland*

[1] *Now at Department of Physics, University of Barcelona, Spain*
[2] *Now at Department of Physics, University of Washington, Seattle (WA), USA.*

Abstract

During the past seven years, the DREAM Collaboration has systematically investigated all factors that determine and limit the precision with which the properties of hadrons and jets can be measured in calorimeters. Using simultaneous detection of the deposited energy and the Čerenkov light produced in hadronic shower development (*dual readout*), the fluctuations in the electromagnetic shower fraction could be measured event by event and their effects on signal linearity, response function and energy resolution eliminated. Detailed measurement of the time structure of the signals made it possible to measure the contributions of nuclear evaporation neutrons to the signals and thus reduce the effects of fluctuations in "invisible energy".
We are now embarking on the construction of a full-scale calorimeter which incorporates all these elements and which should make it possible to measure the four-vectors of both electrons, hadrons and jets with very high precision, in an instrument that can be simply calibrated with electrons.
We request CERN's support for this project in the form of facilities needed to measure the performance of this device.

1 Introduction

DREAM [1], based on an idea proposed in 1997 [1], started in 2002 as a generic detector R&D project, intended to explore (and, if possible, eliminate) the obstacles that prevent calorimetric detection of hadrons and jets with a comparable level of precision as we have grown accustomed to for electrons and photons. The initial collaboration, consisting of fewer than 10 physicists, built a prototype detector (the Dual-Readout Module) at Texas Tech University, which was shipped to CERN and successfully tested at the SPS in 2003 and 2004. The excellent results obtained in these tests generated a lot of interest, and the collaboration has considerably expanded since that time.

In these early tests, we concentrated on the dominating source of fluctuations, *i.e.* fluctuations in the electromagnetic content of hadron showers. After these initial studies, in which the effects of these fluctuations on hadronic calorimeter performance were successfully eliminated, the collaboration has focused on the remaining effects, which rose to prominence as a result: Sampling fluctuations, signal quantum statistics and nuclear breakup effects.

In this context, we have also carried out (in 2006-2009) a series of successful studies of crystal calorimeters, and of methods to split the signals from these crystals into scintillation and Čerenkov components. Recently, a full-size crystal matrix consisting of 100 BGO crystals served as the em section of a hybrid calorimeter system, in which the original fiber calorimeter formed the hadronic section.

The results of these, and many other studies of all aspects of the limitations of hadronic calorimeter performance that have been carried out by the DREAM collaboration from 2003-2009 are described in 17 papers in the refereed literature. These are listed in Section 3.6.

Even though DREAM has always been in essence a generic R&D project, several collaboration members have of course practical applications in mind. These applications include a detector for an experiment at a future Linear e^+e^- Collider in the TeV energy range (ILC, CLIC) [2], and an upgrade of existing calorimeter systems, *e.g.* in the context of SLHC.

The DREAM project has been carried out in a phased manner. That also applied to the funding. At each stage, we have set new goals, based on what was learned during the previous stage. In the period 2002 - 2009, funding for the different stages of this project was received from the US department of Energy (through the ADR program), the State of Texas (ARP program), Texas Tech University and INFN (Gruppo V).

We have now reached the point where we believe that we have all the ingredients in hand to build the perfect calorimeter system, or at least a calorimeter system that meets and exceeds the performance requirements of experiments at the ILC and CLIC. We have proposed to prove this statement by building and testing such a detector to our funding agencies, which have responded favorably. We have received $540K in FY09/10 funds from the US Department of Energy, and the Italian Ministry of Universities and Research, together with the participating Italian universities, have allocated €370K. Substantial support from INFN comes in the form of workshop time, crucial for the construction of the detectors. Work on the construction of this new detector has started.

This document is organized as follows. The ideas on which DREAM calorimeters are based

[1] The name DREAM stands for Dual-REAdout Method.

are described in Section 2 and a selection of crucial experimental results is presented in Section 3. Details of our proposed plans for the final phase of the DREAM project are described in Section 4. The support requested from CERN is discussed in Section 5. Concluding remarks are given in Section 6.

2 The DREAM approach to ultimate calorimetry

The energy resolution of calorimeters is determined by fluctuations. If one wants to improve that resolution significantly, then one has to address the dominating source of these fluctuations. In almost all calorimeters (*i.e.* the ones with $e/h \neq 1.0$), fluctuations in the electromagnetic shower fraction ($f_{\rm em}$) dominate the energy resolution for hadrons and jets. These fluctuations, and their energy dependence, are also responsible for other undesirable calorimeter characteristics, in particular hadronic signal non-linearity and a non-Gaussian response function. There are two possible approaches to eliminate (the effects of) these fluctuations [3]: By designing the calorimeter such that the response to em and non-em energy deposit is the same (compensation, $e/h = 1.0$), or by measuring $f_{\rm em}$ event by event. The DREAM project follows the latter approach. Therefore, calorimeters built according to the DREAM principles are *not* subject to the limitations imposed by the requirements for compensating calorimetry: A small sampling fraction (and the corresponding large sampling fluctuations), and the need to integrate the signals over a very large detector volume (because of the crucial signal contributions of soft neutrons).

2.1 The unique benefits of Čerenkov light

Calorimeters based on Čerenkov light as the signal source are, for all practical purposes, only responding to the em fraction of hadronic showers [4]. This is because the electrons/positrons through which the energy is deposited in the em shower component are relativistic down to kinetic energies of only ~ 200 keV. On the other hand, most of the non-em energy in hadron showers is deposited by non-relativistic protons generated in nuclear reactions [3]. However, in other types of active media (scintillator, LAr) such protons do generate signals. The DREAM detector uses two active media, hence the name (dual-readout): Scintillating fibers measure dE/dx, while clear fibers measure the Čerenkov light generated in the shower development. By comparing the two signals, $f_{\rm em}$ can be measured event by event, and the total shower energy can be reconstructed using the known e/h value(s) of the calorimeter.

We have demonstrated experimentally that this principle works very well [5]. Figure 1 shows the Čerenkov signal distribution for 100 GeV π^- showers (top diagram), as well as the signal distributions for event samples selected for 3 bins of the em shower fraction (bottom diagram). The larger the value of $f_{\rm em}$, the larger the calorimeter signal. The overall signal distribution (top) is evidently a superposition of many narrow distributions such as the ones in the bottom diagram. By using the measured value of $f_{\rm em}$, the total signal distribution can be transformed into a narrow one, with the correct central value, *i.e.* the signal one would find for pure em showers of the nominal energy. This is illustrated in Figure 2, which concerns the signal distributions from 200 GeV multiparticle events (reaction products from an upstream target, intended to mimick jets).

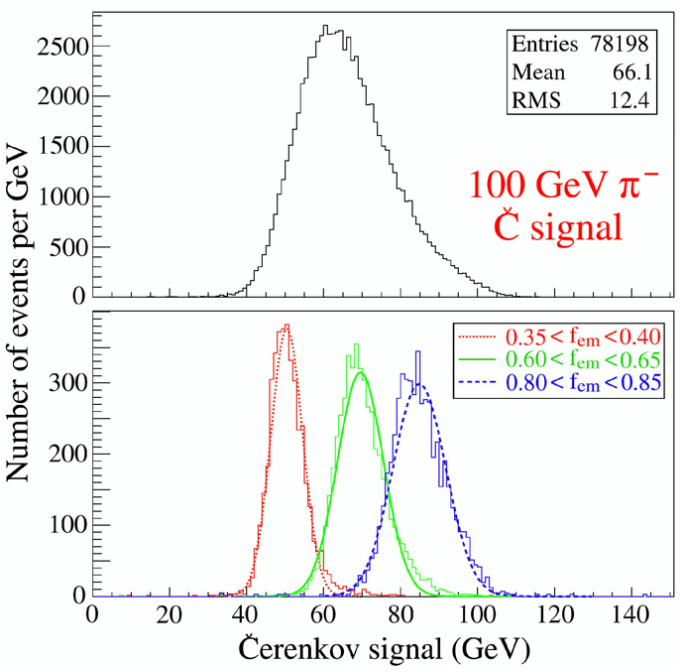

Figure 1: Čerenkov signal distributions for 100 GeV π^-. Shown are all events (top) and samples selected on the basis of their electromagnetic shower content (bottom) [5].

The raw Čerenkov signal distribution (Figure 2a) shows the usual characteristics: Asymmetric, broad and a central value that is much too small (133 GeV). After applying the correction method based on event-by-event measurements of $f_{\rm em}$, this distribution is transformed into the one shown in Figure 2b, which is almost perfectly symmetric, much more narrow, and centered around approximately the correct energy value (190 GeV). It should be emphasized that the value of $f_{\rm em}$ was uniquely determined on the basis of the *ratio* of the two measured signals (the so-called Q/S method [2]), no other information was used. Because of the relatively small detector size (1200 kg), this result is dominated by fluctuations in (lateral) leakage. We have demonstrated that, by using knowledge of the total shower energy, this effect could be eliminated and the signal distribution improved to the one shown in Figure 2c.

2.2 Further improvements

The beam tests of the DREAM fiber detector have shown that, simply by using the ratio of the Čerenkov and scintillation signals, all detrimental effects of fluctuations in the em shower fraction could be eliminated: Hadronic signal linearity was restored, deviations from $E^{-1/2}$ scaling in the hadronic energy resolution were eliminated, a Gaussian response function was obtained and, most importantly, the hadronic energy scale was the same as the electromagnetic one, so that the entire instrument could be calibrated with electrons [5].

The elimination of (the effects of) this dominant source of fluctuations meant that other types of fluctuations now dominated the detector performance. Further improvements should

[2]The symbol Q refers to the quartz fibers that measured the Čerenkov light.

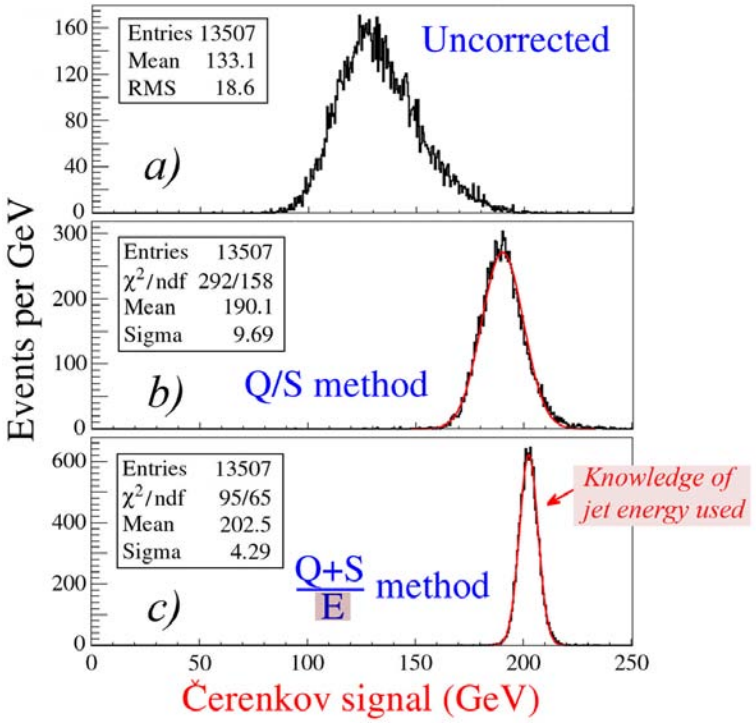

Figure 2: Čerenkov signal distributions for 200 GeV multi-particle events. Shown are the raw data (a), and the signal distributions obtained after application of the corrections based on the measured em shower content, with (c) or without (b) using knowledge about the total "jet" energy [5].

be obtained by concentrating on these. Three types of fluctuations dominated and limited the energy resolution of the DREAM fiber calorimeter:

1. Leakage fluctuations
2. Fluctuations in the Čerenkov light yield
3. Sampling fluctuations

The first source can be eliminated by making the detector sufficiently large. The tested instrument had an effective radius of only 0.8 $\lambda_{\rm int}$. Side leakage amounted, on average, to about 10% of the shower energy, and fluctuations in this fraction played a dominant role. In the new, full-scale detector we are now building these fluctuations will be reduced to negligible proportions. More details on this important point are given in Section 4.1.

Fluctuations in the small number of Čerenkov photons (8 photoelectrons per GeV in the quartz fibers) contributed more than $35\%/\sqrt{E}$ to the measured hadronic energy resolution. Sampling fluctuations were measured to contribute $\sim 20\%/\sqrt{E}$ to the electromagnetic resolution of the detector, and were estimated to contribute about twice as much to the hadronic energy resolution. Also the effects of these sources of fluctuation will be considerably reduced in the new detector.

There is absolutely no reason why the DREAM principles should be limited to fiber calorimeters. In particular, they could be applied to *homogeneous* detectors, provided that a way

was found to distinguish the Čerenkov and scintillation light produced by such detectors. If successful, this approach could eliminate at once both the effects of sampling fluctuations and the effects of fluctuations in the Čerenkov light yield to the hadronic energy resolution. For this reason, the DREAM Collaboration has since 2006 carried out a variety of studies involving crystal calorimeters.

In order to distinguish the contributions from the Čerenkov and the (dominating) scintillation components to the crystal signals, we have exploited three properties:

1. The Čerenkov light is *directional*, while the scintillation light is isotropically emitted. By reading out the detector from two opposite sides, and by varying the detector *orientation*, a contribution of Čerenkov light manifests itself as an angle-dependent asymmetry.

2. The Čerenkov light is *prompt*, whereas the scintillation processes in the crystals exhibit one or several decay constants. By measuring the detailed time structure of the signals, the two components of the signal may be distinguished.

3. The two types of light have *different spectra*. Whereas each scintillating agent has its own unique spectral features, the spectrum of the Čerenkov light exhibits a characteristic λ^{-2} shape. If these two spectra are sufficiently different, they can be separated by means of optical filters.

An additional feature that potentially also might be used to distinguish the contributions of the two types of light to the calorimeter signals is the fact that Čerenkov light is polarized. We have not exploited this aspect.

Figure 3 illustrates the effects of all three methods mentioned above, for measurements carried out on a $PbWO_4$ crystal doped with 1% molybdenum [6]. The experimental setup is shown in Figure 3a. A beam of 50 GeV electrons was steered through the center of this crystal, which was placed on a platform that could rotate around a vertical axis. The angle θ between the crystal axis and the plane perpendicular to the beam line could be varied between -50° and 50°. In the geometry shown in the figure, $\theta \approx -20^\circ$. Trigger counters (TC) and drift chambers (DC) allowed us to measure the passage and the trajectory of the beam particles, respectively. The signals generated by the beam particles traversing this crystal were read out with PMTs from both sides. One side (labeled R) was equipped with a UV optical transmission filter, the other side (labeled L) with a yellow filter. The PMT signals were digitized with a fast sampling oscilloscope, which measured the amplitude of the signals every 0.8 ns. The (average) time structures of the two signals measured this way are depicted in Figure 3b. These signals are very different. The UV signal is prompt, whereas the yellow signal exhibits an exponential decay with a time constant of 26 ns. The fact that the UV signals are caused by Čerenkov light and the yellow signals by scintillation light is further illustrated by the angular dependence of the signal ratio (integrated over the entire time structure), which is shown in Figure 3c. This ratio is strongly dependent on the angle of incidence and reaches a maximum near $\theta = 27^\circ$, *i.e.* precisely where one would expect the Čerenkov signal to reach a maximum, since Čerenkov light is emitted at an angle of 63° by ultra-relativistic particles traversing this crystal (index of refraction $n = 2.2$).

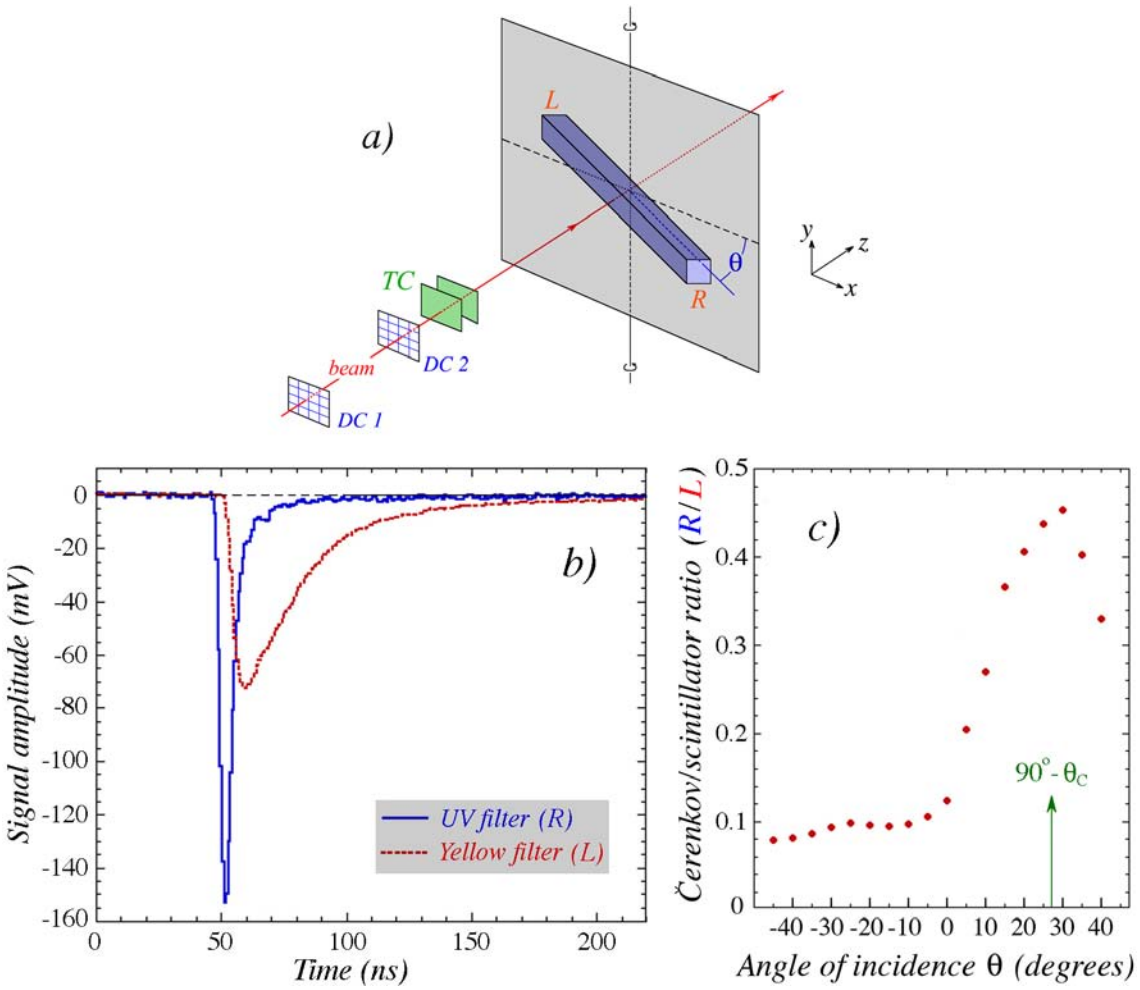

Figure 3: Unraveling of the signals from a Mo-doped $PbWO_4$ crystal into Čerenkov and scintillation components. The experimental setup is shown in diagram a. The two sides of the crystal were equipped with a UV filter (side R) and a yellow filter (side L), respectively. The signals from 50 GeV electrons traversing the crystal are shown in diagram b, and the angular dependence of the ratio of these two signals is shown in diagram c. More details are given in the text [6].

2.3 Toward ultimate calorimetry

If the dual-readout principles could be as efficiently applied in homogeneous detectors as in the original DREAM calorimeter, then the contributions of signal quantum fluctuations and sampling fluctuations to the hadronic energy resolution can be made negligibly small. This means that the factors that dominated and limited the energy resolution of compensating calorimeters (SPACAL, ZEUS) to (the current world record of) $\sim 30\%/\sqrt{E}$ could be reduced to insignificant levels in this type of calorimeter. As illustrated in Section 4, we have reason to believe that this is the case.

The resolution of a sufficiently large detector would then become dominated by *nuclear breakup* effects. Fluctuations in the fraction of the total energy needed to release protons, neutrons and heavier nuclear fragments in the nuclear reactions initiated by the shower particles

lead to fluctuations of the *visible energy*, and thus to fluctuations in the calorimeter response. It has been demonstrated previously [7] that a measurement of the total kinetic energy carried by neutrons generated in the shower development is a powerful tool for reducing the effects of these fluctuations, especially in high-Z absorber materials where most of the nucleons released in the nuclear reactions are indeed neutrons. The contributions of neutrons to the signals are responsible for the fact that the energy resolution of compensating calorimeters based on plastic-scintillator readout is considerably better than in those that use liquid-argon or silicon as active components. Neutron contributions also explain why the energy resolution of compensating calorimeters using uranium as absorber material is not as good as in lead/plastic-scintillator devices, since a large fraction of the neutrons in uranium come from fission, instead of nuclear spallation, and the energy they carry is thus not correlated to the invisible energy losses [3].

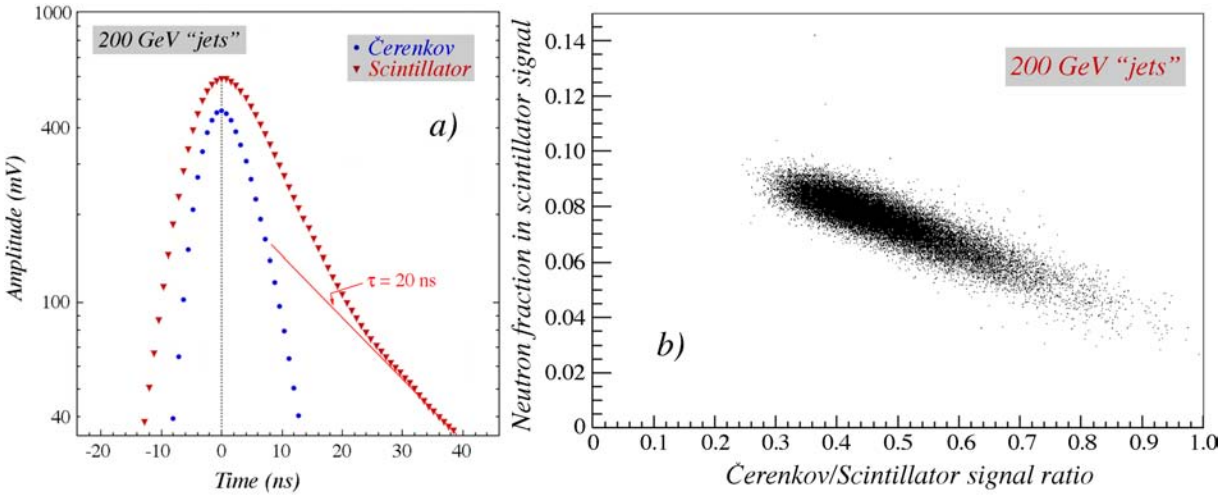

Figure 4: The average time structure of the Čerenkov and scintillation signals recorded for 200 GeV "jets" in the fiber calorimeter (a). Scatter plot of the fraction of the scintillation light contained in the (20 ns) exponentional tail versus the Čerenkov/scintillation signal ratio measured in these events (b) [9].

Measuring the signal contributions from shower neutrons event by event has always been another important objective of the DREAM Collaboration. We have demonstrated that this can be achieved by measuring the time structure of the scintillator signals [8, 9]. The neutron contribution manifests itself as a tail with a characteristic time constant ($\sim$ 20 ns in our fiber calorimeter). As illustrated in Figure 4a, this tail was absent in the Čerenkov signals and also in scintillator signals generated by em showers. The time structure measurements made it possible to determine the relative contribution of this tail to the scintillation signals event by event. The fact that this fraction was anti-correlated with the Čerenkov/scintillation signal ratio (Figure 4b), and thus with the relative strength of the em shower component, underscores that this tail indeed represents the neutrons produced in the shower development [9].

If the techniques described above would be fully exploited for eliminating the effects of the fluctuations that limit the performance of hadron calorimeters, then the theoretical resolution limit of $\sim 15\%/\sqrt{E}$ should be within reach. Dual-readout detectors thus hold the promise of high-quality calorimetry for *all* types of particles, with an instrument that can be calibrated with electrons.

3 Experimental results

In this section, we present some of the highlights of seven years of R&D that form the basis for the present proposal.

3.1 The original DREAM detector

The basic element of our generic prototype detector was an extruded copper rod, 2 meters long and $4\times$ 4 mm^2 in cross section. This rod was hollow, the central cylinder had a diameter of 2.5 mm. In this hole were inserted 7 optical fibers. Three of these were plastic scintillating fibers, the other four fibers were undoped fibers, intended for detecting Čerenkov light. We used two types of fibers for the latter purpose. For the central region of the detector, high-purity quartz fibers were used, while the peripheral regions of the detector were equipped with acrylic plastic fibers. The fiber pattern was the same for all rods, as shown in Figure 5.

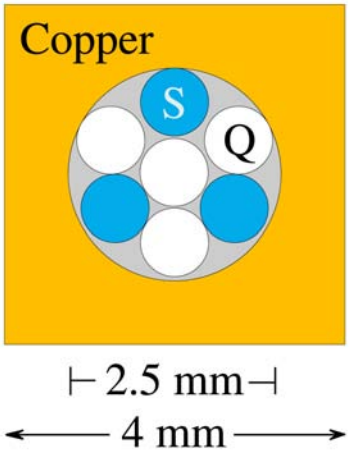

Figure 5: The basic building block of the DREAM detector is a 4 $\times$ 4 mm^2 extruded hollow copper rod of 2 meters length, with a 2.5 mm diameter central hole. Seven optical fibers (4 undoped and 3 scintillating fibers) with a diameter of 0.8 mm each are inserted in this hole, as shown.

The DREAM detector consisted of 5580 such rods, 5130 of these were equipped with fibers. The instrumented volume thus had a length of 2.0 m, an effective radius of 16.2 cm and a mass of 1030 kg. The effective radiation length of the calorimeter was 20.10 mm, the Moliére radius 20.35 mm and the nuclear interaction length 200 mm. The fibers were grouped to form 19 towers. Each tower consisted of 270 rods and had an approximately hexagonal shape (80 mm apex to apex). The effective radius of each tower was thus 37.1 mm ($1.82\rho_M$). A central tower was surrounded by two hexagonal rings, the Inner Ring (6 towers) and the Outer Ring (12 towers). The towers were longitudinally unsegmented.

The fibers sticking out at the rear end of this structure were separated into 38 bunches: 19 bunches of scintillating fibers and 19 bunches of Čerenkov fibers. In this way, the readout structure was established (see also Figure 6b). Each bunch was coupled through a 2 mm air gap to a photomultiplier tube (PMT). In the case of the scintillating fibers, the surface of the PMTs was covered with a yellow filter. Since the dominating blue light from these fibers is

attenuated by self-absorption (resulting from overlap of the emission and absorption bands) this filter increased the light attenuation length of the fibers substantially. In this way, we traded light yield (not critical for the hadronic performance) for longitudinal uniformity. The light attenuation characteristics of the Čerenkov fibers turned out to be adequate without filtering.

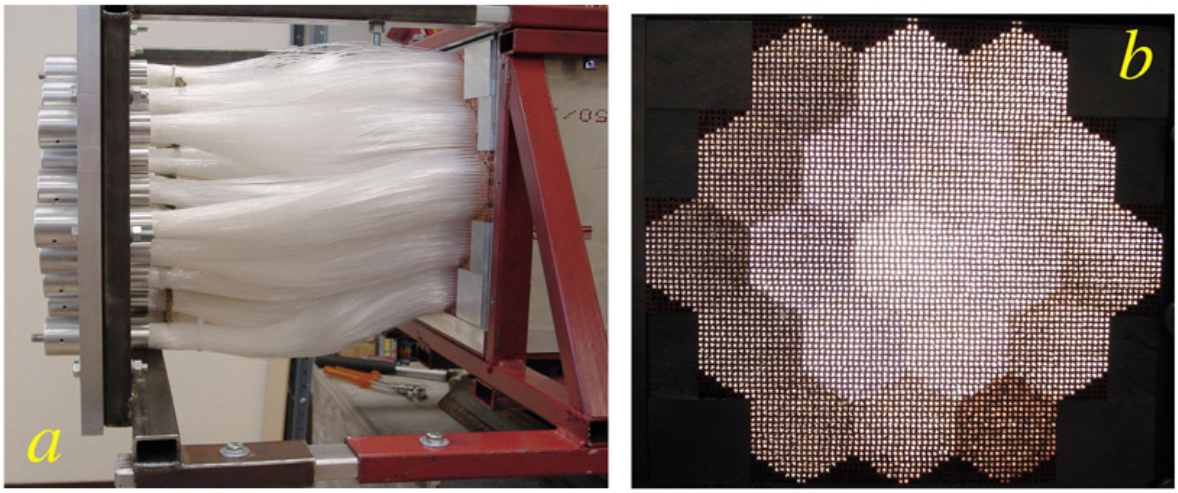

Figure 6: The DREAM detector. Shown are the fiber bunches exiting from the rear face of the detector (a) and a picture taken from the front face while the rear end was illuminated (b). The hexagonal readout structure is made visible this way.

Figure 6 shows pictures of the assembled detector. In Figure 6a, the fiber bunches exiting the downstream end of the calorimeter and the 38 PMTs used to detect their signals are shown. In total, this detector contained about 90 km of optical fibers. Figure 6b shows an image of the front face of the calorimeter, while the forest of fibers sticking out from the back was illuminated with a strong lamp. The hexagonal readout structure is clearly visible in this picture.

3.2 Beam tests

All measurements have been performed in the H4 beam line of the Super Proton Synchrotron at CERN. The fiber calorimeter was mounted on a platform that could move vertically and sideways with respect to the beam. Changing the angle of incidence of the beam particles with respect to the fibers in the horizontal plane (the θ angle) and the tilt angle (ϕ) was achieved with the intervention of a crane. For most of the measurements, these angles were very small, $< 3°$, *i.e.* the particles entered the calorimeter in approximately the same direction as the fibers were oriented. For pions and jets, this angle turned out to be unimportant, but for electromagnetic showers, which especially in their early phase are very narrow, the response function turned out to depend on the impact point (absorber or fiber) when θ, ϕ were very small.

We also performed a series of measurements in which the detector was rotated over an angle $\theta = 24°$. These measurements made it possible to determine the attenuation lengths of the various fiber types. They also provided interesting information about the longitudinal shower profiles, and in particular about differences in these profiles between the scintillator and Čerenkov

measurements [10]. Measurements at $\theta = 90°$ (in which the fibers were oriented perpendicular to the beam direction) provided interesting details about the angular distribution of shower particles contributing to the Čerenkov signals [11].

We used several auxiliary detectors in these beam tests: An upstream preshower detector and a downstream muon counter made it possible to obtain clean samples of the particles we wanted to study. A fiber hodoscope or a set of drift chambers gave us the impact point of the beam particles in the calorimeter event by event.

The detector was exposed to electron beams with energies ranging from 8 - 200 GeV, and π^- beams with energies ranging from 20 - 300 GeV. Since hadron detectors in modern experiments primarily serve to detect jets, we made a special effort to measure the properties of these objects. For these studies, a 10 cm thick polyethylene target was installed upstream of the calorimeter. This target was sandwiched between upstream and downstream scintillation counters. With this setup, nuclear interactions of the beam pions in the target could be selected, by requiring a mip signal in the upstream counter (indicating the passage of a single pion) and a much larger signal in the downstream counter. The latter signal could also be used to estimate the multiplicity of the secondaries produced in this nuclear reaction. The multiparticle events selected in this way are not completely representative for typical jets studied in high-energy colliding-beam experiments. However, for purposes of calorimetry they are nevertheless extremely useful. In the following, we will refer to these measurements as "jet" measurements.

3.3 Results obtained with the fiber calorimeter

The essential aspects of the DREAM principles are illustrated in Figure 7, which shows a graph in which the Čerenkov signals generated by 100 GeV π^- are plotted versus the scintillator signals generated by the same particles [5]. Every event is represented by a dot in this figure. The

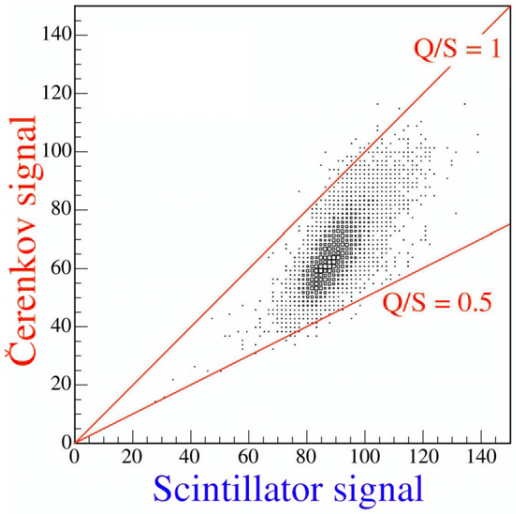

$$Q = E\left[f_{em} + \frac{1}{(e/h)_Q}(1 - f_{em})\right] \quad (1)$$

$$S = E\left[f_{em} + \frac{1}{(e/h)_S}(1 - f_{em})\right] \quad (2)$$

e.g. If $e/h = 1.3$ (S), 4.7 (Q)

$$\frac{Q}{S} = \frac{f_{em} + 0.21\,(1 - f_{em})}{f_{em} + 0.77\,(1 - f_{em})} \quad (3)$$

$$E = \frac{S - \chi Q}{1 - \chi} \quad (4)$$

with $\chi = \frac{1 - (h/e)_S}{1 - (h/e)_Q} \sim 0.3$

Figure 7: Scatter plot of the Čerenkov signals for 100 GeV π^- mesons versus those generated by the scintillating fibers in the DREAM calorimeter. Each event is represented by a dot [5].

fact that these dots do *not* cluster around the diagonal demonstrates that the two signals provide complementary information about the shower development . These signals, Q and S, depend on the energy of the showering particle (E), on the em shower fraction ($f_{\rm em}$) and on the e/h value, which suppresses the response to the non-em shower component (Equations 1,2). The dual-readout method works because the e/h values are very different for the copper/scintillator and copper/Čerenkov fiber structures: 1.3 and 4.7, respectively. Equations 1 and 2 thus can be solved for either of the two unknown quantities, $f_{\rm em}$ or E. If we divide 1 by 2, the shower energy is eliminated and the resulting Equation 3 gives a simple, *energy-independent* relationship between the ratio of the two measured signals and the em shower fraction. A measurement of this ratio thus provides directly the value of $f_{\rm em}$ for each individual event. Events with the same signal ratio are located on a straight line through the bottom left corner of the scatter plot in Figure 7.

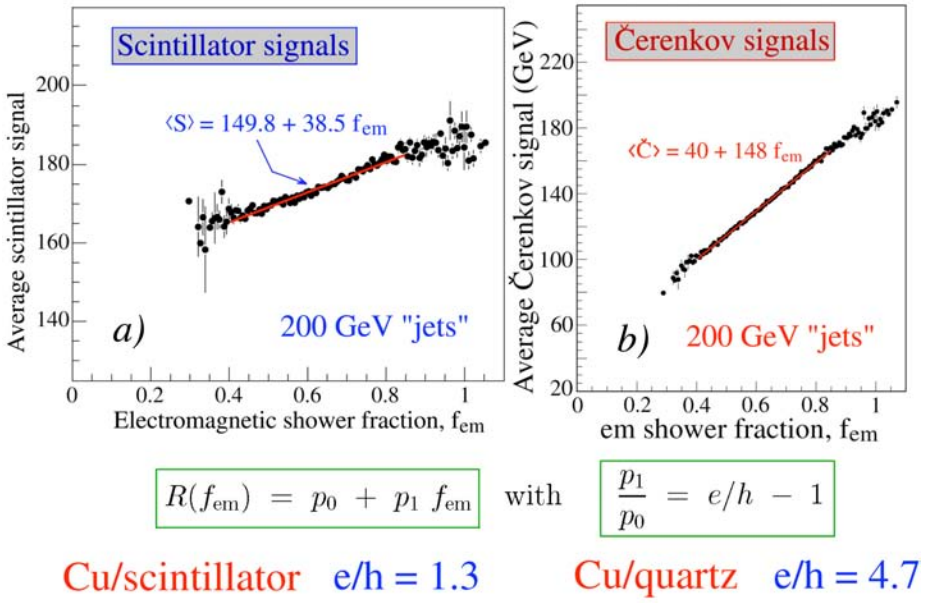

Figure 8: The average scintillator (a) and Čerenkov (b) signals for 200 GeV jets, as a function of the em shower fraction, $f_{\rm em}$ [5].

Figure 8 shows that the measured signal depends indeed linearly on the $f_{\rm em}$ fraction found in this way (see also Figure 1), both for the scintillator and the Čerenkov signals. The slope of these curves provided the precise e/h values mentioned above.

One can also solve Equations 1 and 2 for the shower energy E. This results in Equation 4, which provides a simple recipe to determine that energy for each individual event on the basis of the two measured signals and one constant (χ) characteristic for the calorimeter system. Figure 9a shows that the energy calculated this way is within a few percent equal to the energy of the electrons that were used to calibrate this calorimeter, and that the large hadronic non-linearity, which is typical for non-compensating calorimeters, was almost completely eliminated with this procedure. Other benefits of the dual-readout method included a strongly improved hadronic energy resolution and a Gaussian response function (Figure 2). In addition, the deviations from $E^{-1/2}$ scaling in the hadronic energy resolution almost completely disappeared after the (Q/S)

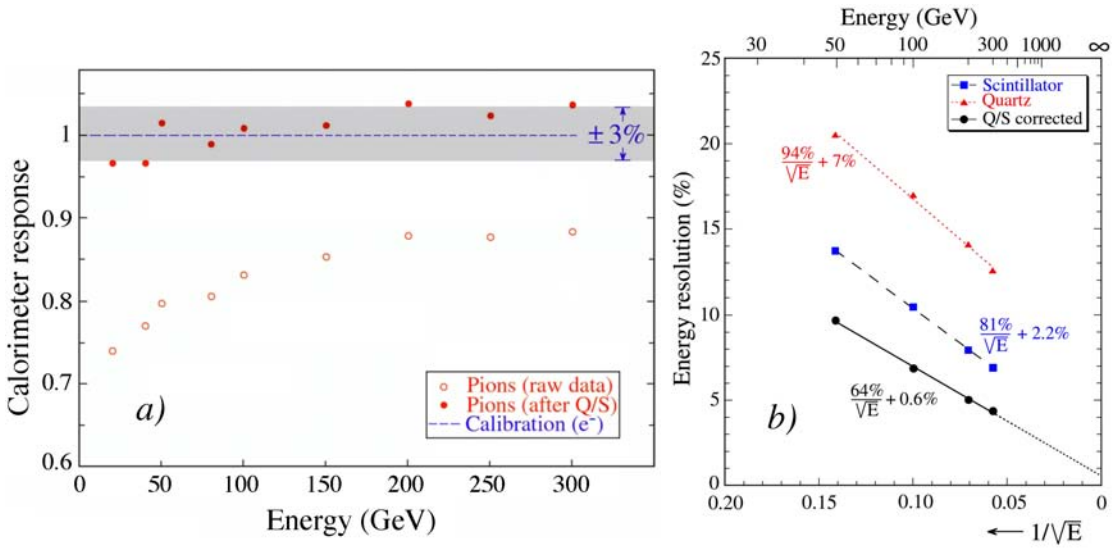

Figure 9: The scintillator response of the DREAM calorimeter to single pions (a) and the energy resolution for "jets" (b), before and after the dual-readout correction procedures were applied to the signals [5].

corrections were applied (Figure 9b). The simple and straightforward correction procedures described above worked not only well for single hadrons, but also for multiparticle "jets".

The tests of the fiber calorimeter thus have demonstrated that the complementary information from dE/dx and from the production of Čerenkov light provides a very powerful tool for improving the hadronic calorimeter performance, and that a detector of this type could provide all the essential advantages of compensating calorimetry, *without* the limitations inherent to compensating calorimeters, *i.e.* a small sampling fraction, large integration cones and relatively long signal integration times.

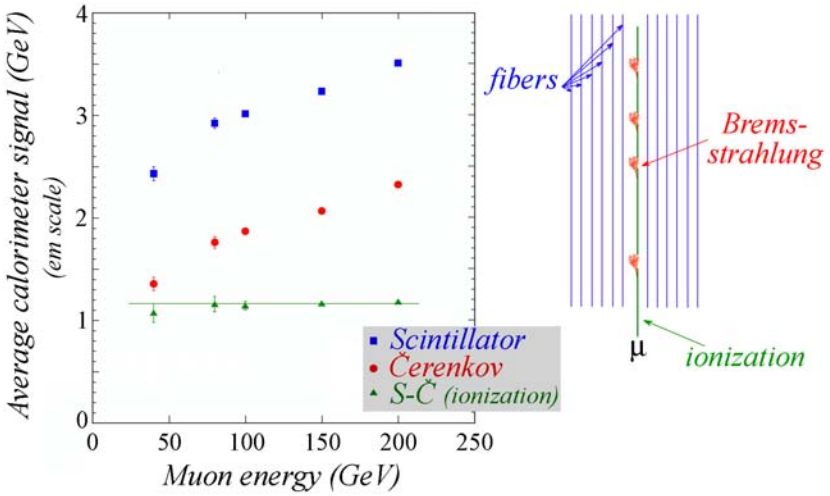

Figure 10: Average values of the scintillator and Čerenkov signals from muons traversing the DREAM calorimeter, as a function of the muon energy. Also shown is the difference between these signals. All values are expressed in units of GeV, as determined by the electron calibration of the calorimeter [12].

Simultaneous detection of the scintillation and Čerenkov light produced in the shower development turned out to have other, unforeseen beneficial aspects as well. One such effect is illustrated in Figure 10, which shows the signals from muons traversing the DREAM calorimeter along the fiber direction [12]. The gradual increase of the response with the muon energy is a result of the increased contribution of radiative energy loss (Bremsstrahlung) to the signals. The Čerenkov fibers are *only* sensitive to this energy loss component, since the primary Čerenkov radiation emitted by the muons falls outside the numerical aperture of the fibers. The constant (energy-independent) difference between the total signals observed in the scintillating and Čerenkov fibers represents the non-radiative component of the muon's energy loss. Since both types of fibers were calibrated with em showers, their response to the radiative component is equal. This is the only example we know of a detector that separates the energy loss by muons into radiative and non-radiative components.

3.4 Homogeneous DREAM detectors

Once the benefits of simultaneous detection of scintillation and Čerenkov light were clearly established, the DREAM project moved into the next phase, in which we concentrated on the following question: " Is it possible to apply the dual-readout principles to detectors in which the scintillation and the Čerenkov light are generated in *one and the same light producing medium*?" An affirmative answer to this question would be important for two reasons:

1. The effects of sampling fluctuations and (Čerenkov) photoelectron statistics, which would dominate the hadronic resolution of a sufficiently large fiber detector, could be greatly reduced in this way.

2. It could then become possible to build calorimeter systems that would not only have very good performance for hadrons and jets, but also have excellent electromagnetic resolution.

In general, calorimeter systems have a separate em section, optimized for electron and photon detection. Such a section is typically $\sim 1\lambda_{\rm int}$ deep and absorbs half of the energy carried by jets. Application of the dual-readout principles in such a segmented calorimeter system would only make sense if one could also detect both dE/dx and Čerenkov signals from the em calorimeter section. Crystals producing a mixture of scintillation and Čerenkov light would provide that option.

The feasibility of this was studied in two steps. First, we modified the readout of the existing fiber calorimeter. In a limited region of the detector, the two types of fibers were connected to the same PMT. This made it possible to study the benefits (or lack thereof) of several of the methods listed in Section 2.2 for unraveling the mixed scintillator/Čerenkov signals created in this way [13]. The information gained in this process was later used in our studies of the performance of crystals as dual-readout calorimeters.

Not surprisingly, we found that the separation of the calorimeter signals into Čerenkov and scintillation components worked best if the contributions of both components to the signal were of comparable strength. Therefore, our search for appropriate crystals focused initially on poor scintillators with high Z values. Lead tungstate ($PbWO_4$), the crystal of choice in several modern experiments, seemed to be a logical choice.

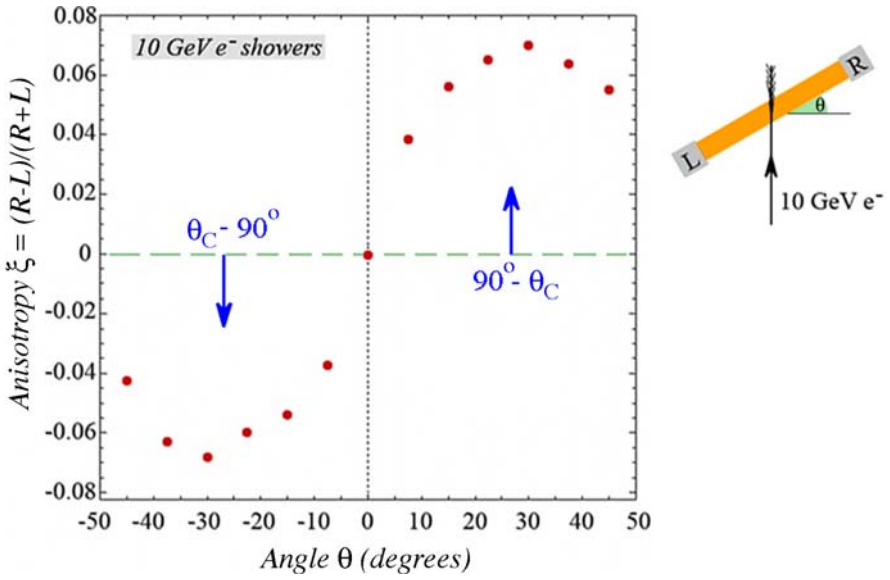

Figure 11: Left-right response asymmetry measured for 10 GeV electrons showering in a $2.5X_0$ thick $PbWO_4$ crystal, as a function of the orientation of the crystal (the angle θ) [14].

Figure 11 provides the proof that a significant fraction, $\sim 15\%$, of the response of this crystal to high-energy particles is indeed due to Čerenkov light [14]. The crystal, read out from both ends with PMTs, was placed in a 10 GeV electron beam, as shown. Any Čerenkov light produced by the showering particles would be emitted at a characteristic angle of $\sim 63^\circ$ with the beam direction. Detection of this light would thus depend on the crystal orientation, *i.e.* on the angle θ. On the other hand, detection of the isotropically emitted scintillation light would be independent of θ. The figure shows a very clear *anisotropy* in the angular dependence of the signals from this crystals. The ratio $(R-L)/(R+L)$ reached its maximum and minimum values near the angles expected for Čerenkov light, $\theta = 27^\circ$ and -27°, respectively.

An alternative way to visualize the Čerenkov component is by comparing the time structure of the signals from this crystal for different angles of incidence. Figure 12 shows the average time structure of the signals measured on the left side (L) of the crystal, for two different orientations of the crystal, as well as the difference between these two time distributions. At $\theta = -30^\circ$, Čerenkov light contributed to the signals, at $\theta = 30^\circ$, it did not [14, 15]. When the crystal was read out from the other side, the prompt excess signal was detected for $\theta = 30^\circ$, and was absent for $\theta = -30^\circ$. Also these results indicated that $\sim 15\%$ of the signal measured at -30° derived from Čerenkov light [15].

These measurements were carried out with a fast digital oscilloscope, which provided a sampling capability of 5 GSample/s, at an analog bandwidth of 2.5 GHz, over 4 input channels. The excellent time resolution provided by this instrument was crucial for separating the prompt Čerenkov component [3] from the scintillation signals, which exhibited an exponential decay with a time constant of less than 10 ns.

[3]The width of the Čerenkov pulse (4 ns FWHM) was the result of instrumental effects, such as fluctuations in PMT transit time, effects of the 45 m long cables between the detector and the counting room on the pulses, *etc.*

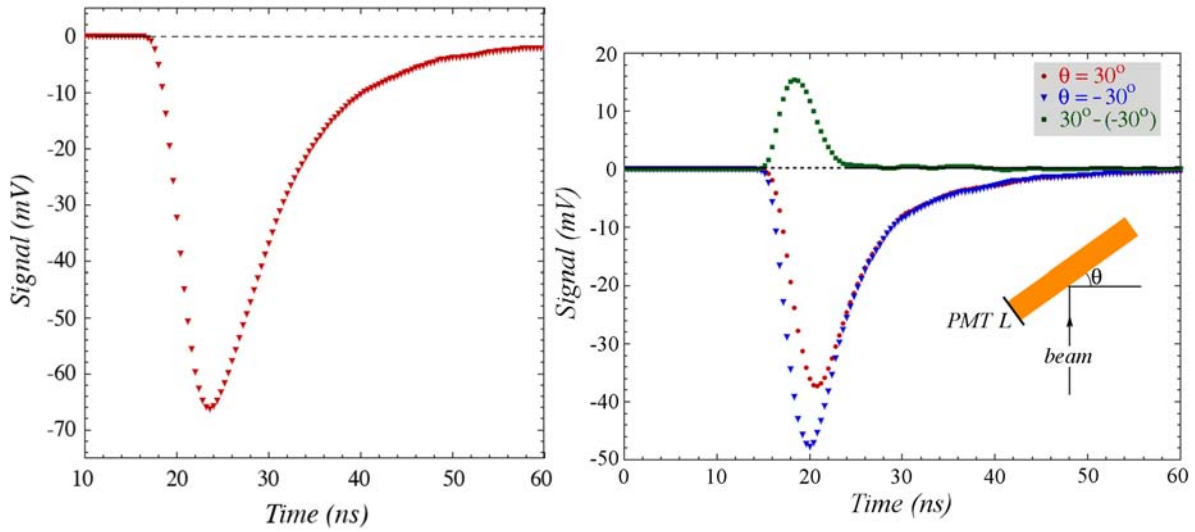

Figure 12: Average time structure of the signals measured with the PMT reading out one end (L) of a $PbWO_4$ crystal traversed by 10 GeV electrons, for two different orientations of the crystal, and the difference between these two time distributions. At $\theta = -30°$, Čerenkov light contributes to the signals, at $\theta = 30°$, it does not [14, 15]. When the crystal was read out from the other side, the prompt excess signal was detected for $\theta = 30°$, and was absent for $\theta = -30°$ [15].

In subsequent measurements, we found that the relative strength of the Čerenkov component of the $PbWO_4$ signals depended strongly on the ambient temperature. This is illustrated in

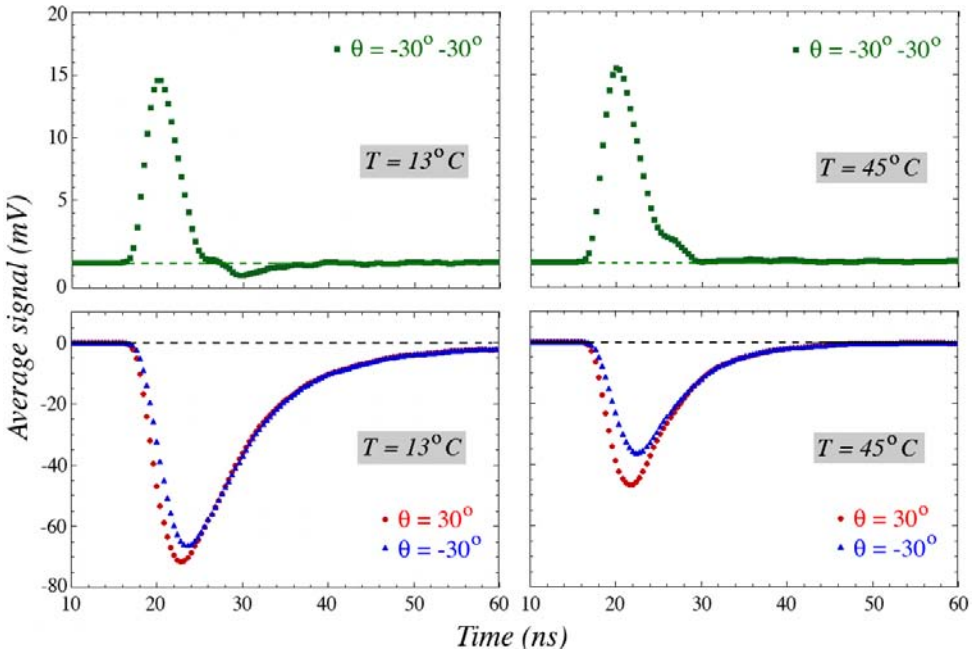

Figure 13: Average time structure of the signals from PMT R measured for 50 GeV electrons traversing the $PbWO_4$ crystal at $\theta = 30°$ and $\theta = -30°$ (*top* plots), as well as the difference between these two signals (*bottom* plots), measured for two different temperatures: 13°C (*left*) and 45°C (*right*) [16].

Figure 13, which shows the signals measured at $\theta = \pm 30^\circ$ for temperatures of 13°C and 45°C, respectively. The total light yield changed by about a factor of two over this temperature range, but this change was entirely due to the scintillation component. The amount of Čerenkov light turned out to be temperature independent in these measurements. We also found that the decay time of the scintillation process decreased significantly when the temperature was raised [16]. Raising the temperature would therefore increase the relative contribution of the Čerenkov component, but the reduced decay time (< 6 ns at $T > 40^\circ$C) would make it very hard to separate the two types of light.

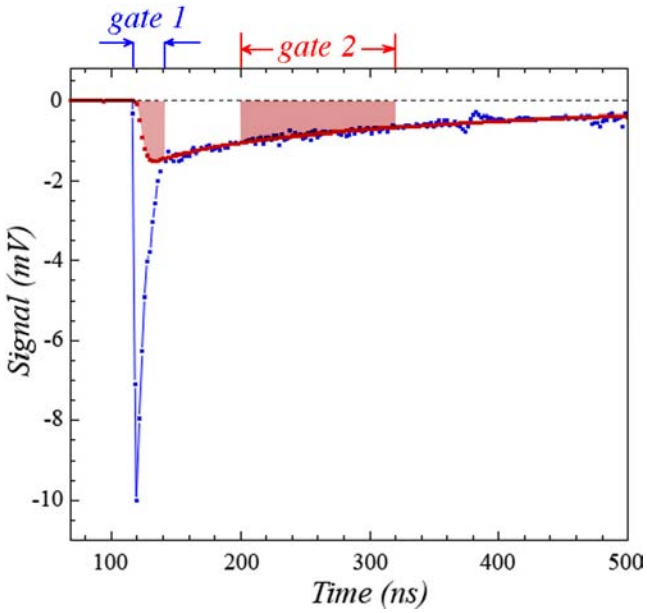

Figure 14: The time structure of a typical shower signal measured in the BGO em calorimeter equipped with a UV filter. These signals were measured with a sampling oscilloscope, which took a sample every 0.8 ns. The UV BGO signals were used to measure the relative contributions of scintillation light (gate 2) and Čerenkov light (gate 1) [15].

Interesting experimental opportunities were found in a totally different type of crystal, bismuth germanate (BGO). Even though Čerenkov radiation represents a much smaller fraction of the light produced by these crystals, it is easier to separate and extract it from the signals. The much longer scintillation time constant and the spectral difference are responsible for that [4]. Figure 14 shows the average time structure of shower signals in a BGO crystal equipped with a UV optical transmission filter. The "prompt" component observed in this signal is due to Čerenkov light, while the slow component (time constant 300 ns) represents the small fraction of the scintillation light that passed through the filter. This was concluded from the fact that the ratio of both signal components changed as a function of the angle of incidence of the beam particles, and reached a maximum when the photons emitted at the Čerenkov angle ($\theta_C = \arccos 1/n \approx 63^\circ$) traveled along the longitudinal crystal axis: $\theta = 27^\circ$ [15].

This type of time structure offers the possibility to obtain all needed information from *only one* signal. An external trigger opens two gates: one narrow (10 ns) gate covers the prompt com-

[4]The BGO scintillation spectrum peaks at 480 nm, while Čerenkov light exhibits a λ^{-2} spectrum.

ponent, the second gate (delayed by 30 ns and 50 ns wide) only contains scintillation light. The latter signal can also be used to determine the contribution of scintillation to the light collected in the narrow gate. In this way, the Čerenkov/scintillation ratio could be measured event-by-event on the basis of one signal only .

Figure 15: The calorimeter during installation in the H4 test beam, which runs from the bottom left corner to the top right corner in this picture. The 100-crystal BGO matrix is located upstream of the fiber calorimeter, and is read out by 4 PMTs on the left (small end face) side. Some of the leakage counters are visible as well (a). The location and numbering of the PMTs reading out the BGO crystal matrix (b) [17].

We have tested this principle in a series of measurements in which the fiber calorimeter was preceded by an electromagnetic section consisting of 100 BGO crystals recovered from the L3 experiment. Due to the fact that we had only four channels available for measuring the time structure of the signals from this crystal matrix, these signals were read out from the side by means of four 3" PMTs (Figure 15). This readout structure was of course far from ideal, since the total photocathode surface area was a factor of four smaller than the surface area through which the light exited from the crystals. In addition, there was no optical contact between these PMTs and the high-n crystals, which severely reduced the size of the signals, and resulted

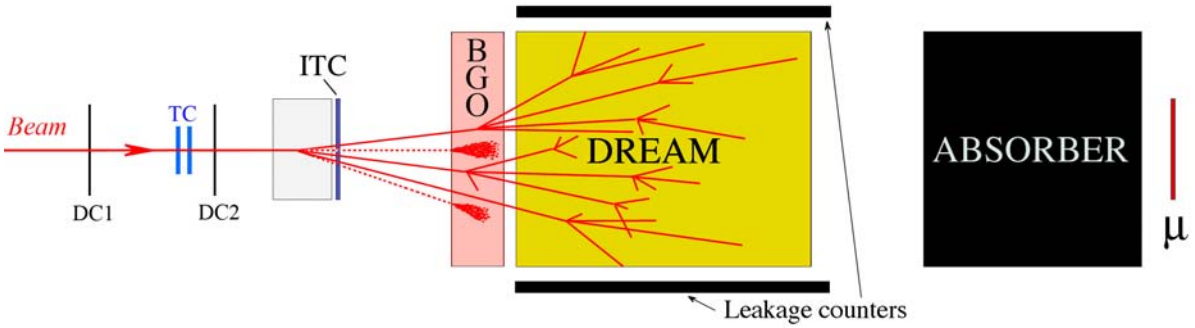

Figure 16: Schematic of the experimental setup in the beam line in which the hybrid calorimeter system was tested (see text for details). Also shown is the occurrence and development of a multi-particle event ("jet") originating in the upstream target [17].

in large non-uniformities. Nevertheless, these measurements were very useful for testing the applicability of the dual-readout techniques in this hybrid calorimeter system.

In order to maximize the sensitivity to the performance of the crystal matrix, these measurements were carried out with multi-particle "jets". The experimental setup is shown in Figure 16. Interactions of the beam particles in the upstream target were selected by requiring a signal of at least 10 times that of a minimum-ionizing particle in the scintillation counter (ITC) placed directly downstream from that target. In events induced by 200 GeV beam pions, about half of the total shower energy was deposited in the (1 λ deep) crystal section of the calorimeter system with this trigger. The signals from this crystal matrix were split into Čerenkov and scintillation components based on the time structure measured with the four PMTs [17].

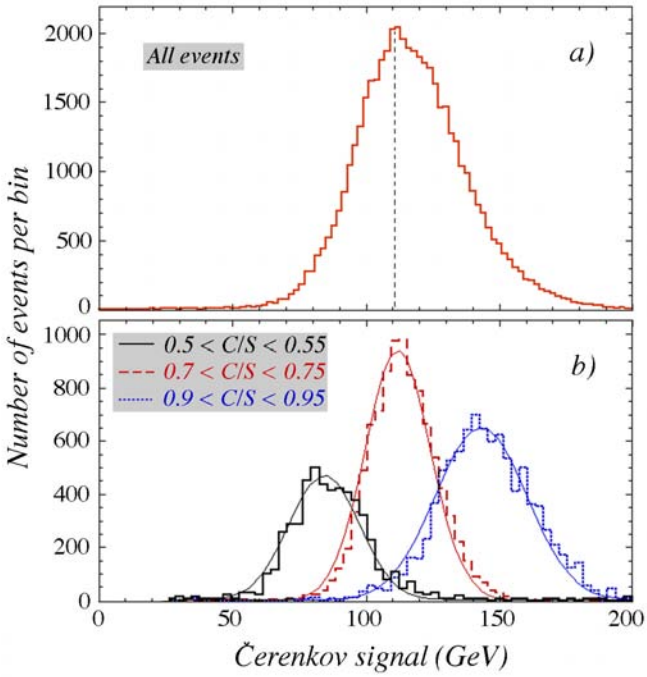

Figure 17: The Čerenkov signal distribution for 200 GeV "jet" events detected in the BGO + fiber calorimeter system (a) together with the distributions for subsets of events selected on the basis of the ratio of the total Čerenkov and scintillation signals in this detector combination (b) [17].

Figure 17 demonstrates that the dual-readout principle also worked well for this hybrid calorimeter system. The figure shows the total (*i.e.* BGO + fiber) Čerenkov signal distribution for the 200 GeV "jet" events (Figure 17a), as well as the signal distributions for event samples selected for three bins of the Čerenkov/signal ratio (Figure 17b). The larger this ratio, the larger the overall calorimeter signal. The overall, asymmetric signal distribution is evidently a superposition of many more narrow, Gaussian distributions such as the ones shown in Figure 17b. This is the same result as we found for the dual-readout fiber operated in stand-alone mode (see Figure 1). We have demonstrated that the widths of the signal distributions of the subsamples, and thus of the overall signal distribution that resulted from the correction procedure was completely dominated by the inadequacies of the readout structure used in these tests. But the validity of the dual-readout principles for a calorimeter with a BGO ECAL was evident from these results.

Apart from these tests with crystals that were readily available, we have also embarked on a separate program to develop a new type of crystal optimized for our purpose. The first results of this effort have just been published [6]. An example is shown in Figure 3, and the results are very encouraging. This coming summer, we are planning to test crystals from the next iteration, which are currently being produced.

3.5 The nuclear neutron component of hadron showers

The detailed measurements of the time structure of the calorimeter signals also proved to be invaluable for dealing with the fluctuations in visible energy caused by nuclear breakup effects. Due to the fact that our oscilloscope only had four channels for measuring this time structure, we had to improvise here as well, by adding the analog signals from different towers of the fiber calorimeter together and digitizing the summed signals. However, since the effects are in this case appearing in the trailing edge of the signals, this was not such a critical issue as for the BGO calorimeter, where a very narrow prompt component provided the crucial information.

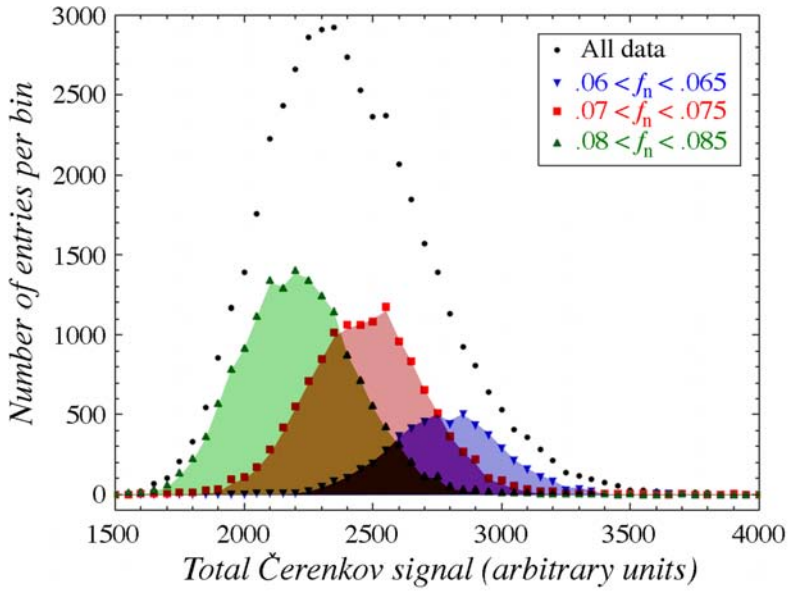

Figure 18: Distribution of the total Čerenkov signal for 200 GeV "jets" and the distributions for three subsets of events selected on the basis of the fractional contribution of neutrons to the scintillator signal [9].

In Figure 4, some essential results of these studies were already shown. It turned out that the neutrons, which provide valuable event-by-event information about the nuclear binding energy losses, manifest themselves as an exponential tail in the time structure of hadronic scintillator signals. As one should expect, the relative contribution of this tail to the total scintillator signal was anti-correlated with the em shower fraction.

Despite the fact that no effort was made to measure this relative fraction with great precision, the results of this study were very valuable for assessing the impact of this additional information on the calorimeter performance. Figure 18 shows the (Čerenkov) signal distribution for 200 GeV

"jets", as well as the signal distributions for three subsamples of events selected on the basis of the relative contribution of neutrons to the scintillator signal [9]. Just as we saw before in Figures 1 and 17, the total signal distribution is a superposition of many narrower, Gaussian distributions. However, the mean values of these subsample signal distributions are in this case determined by the contribution of neutrons to the scintillator signals, not by the em shower fraction. But given the (anti-)correlation between these two quantities (Figure 4b), this should not come as a great surprise.

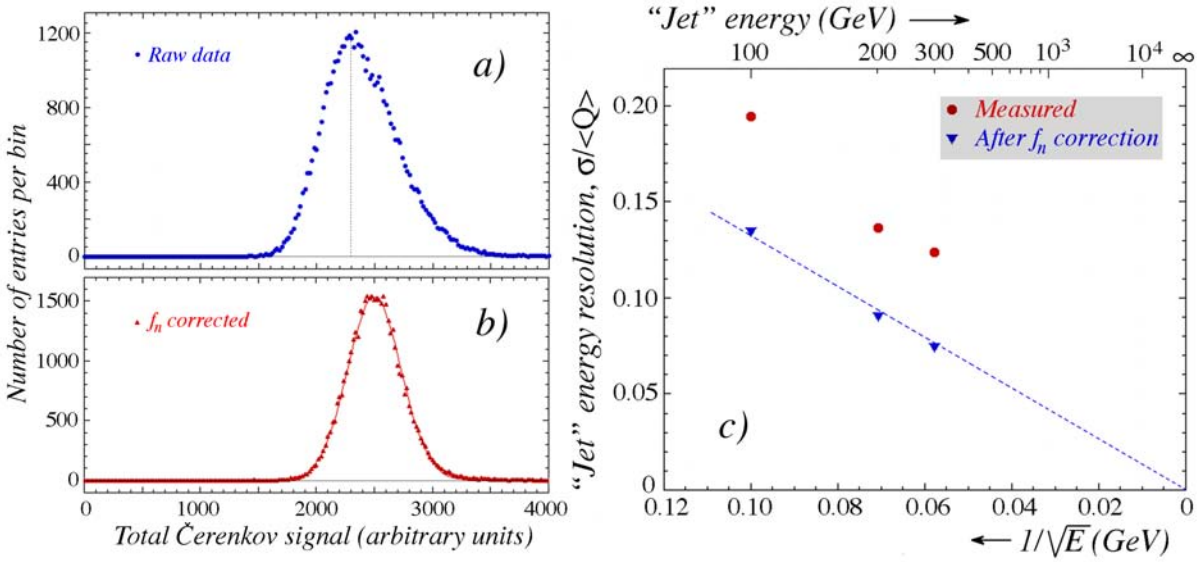

Figure 19: Distribution of the total Čerenkov signal for 200 GeV "jets" before (a) and after (b) applying the correction based on the measured value of f_n, described in the text. Relative width of the Čerenkov signal distribution for "jets" as a function of energy, before and after a correction that was applied on the basis of the relative contribution of neutrons to the scintillator signals (c) [9].

Figure 19 demonstrates that the event-by-event information on the relative contribution of neutrons to the calorimeter signals can be used in similar ways as before to improve the calorimeter performance. For example, this information can be used to make the response function Gaussian (Figure 19b), and in doing so, the non-scaling term in the hadronic energy resolution is eliminated (Figure 19c).

Interestingly, the neutron information described above does **not** require dual-readout calorimetry. One could obtain this information also from a scintillator-based calorimeter, provided that the time structure of the signals is measured. Yet, despite the correlation between the shower fractions carried by the em component ($f_{\rm em}$) and by neutrons (f_n), the information provided by both is complementary.

This is illustrated in Figure 20a, which shows a scatter plot of f_n versus the total Čerenkov signal for two subsamples of 200 GeV "jet" events. All events in each subsample have approximately the same Čerenkov/scintillator signal ratio, *i.e.* the same value of $f_{\rm em}$. However, the fractional neutron contribution to the scintillator signals from the events in each subsample differs quite substantially. Figure 20b shows that the energy resolution is clearly affected by the relative contribution of these neutrons to the signals. As f_n increases, so does the fractional

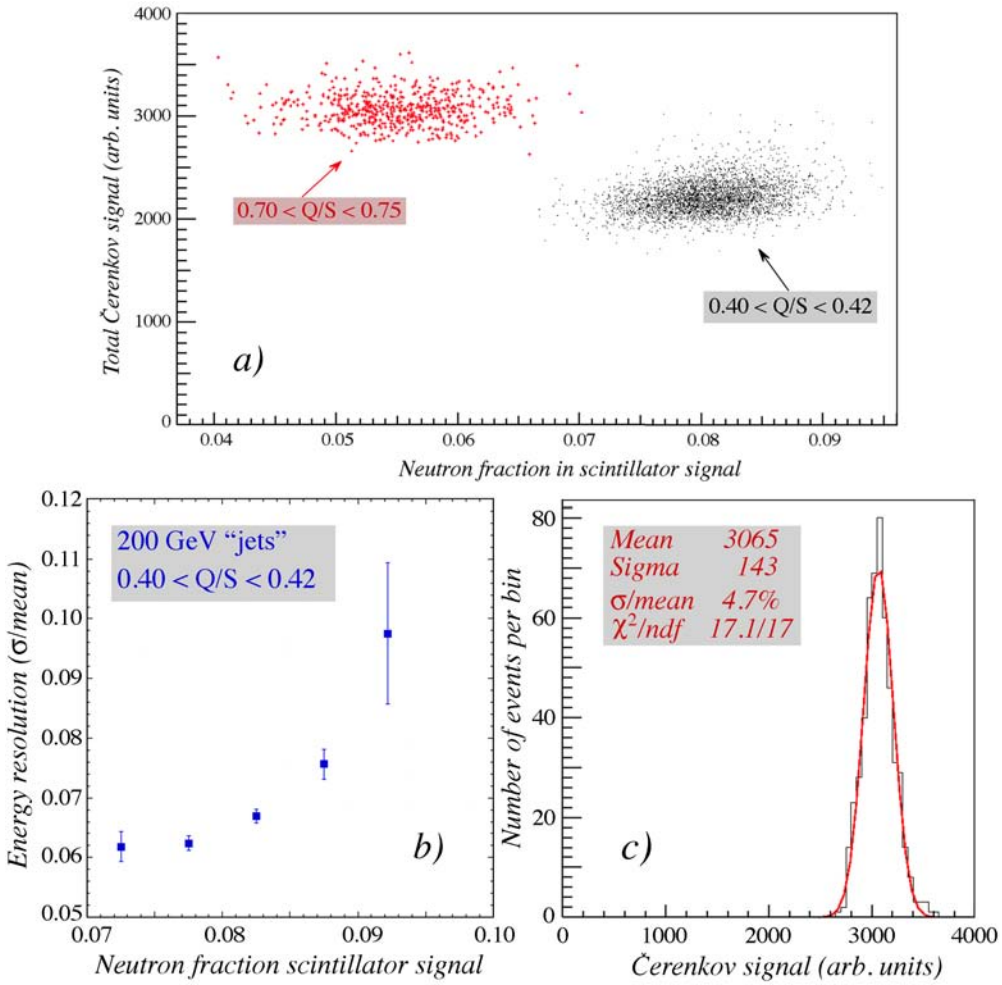

Figure 20: Scatter plot for 200 GeV "jet" events, all of which had either a Q/S signal ratio between 0.40 and 0.42 (the black dots), or between 0.70 and 0.75 (the red crosses). For each individual event, the combination of the total Čerenkov signal and the fractional contribution of neutrons to the total scintillator signal is given (a).The energy resolution for 200 GeV "jets" with the same em shower fraction, as a function of the fractional neutron contribution to the scintillator signals (b). Čerenkov signal distribution for 200 GeV "jets" with $0.70 < Q/S < 0.75$ and $0.45 < f_n < 0.65$, together with the results of a Gaussian fit (c) [9].

width of the Čerenkov signal distribution. A larger $f_n$value means that the average invisible energy fraction is larger. This in turn implies that the event-to-event fluctuations in the invisible energy are larger, which translates into a worse energy resolution, even in signals to which the neutrons themselves do not contribute. Figure 20c illustrates the quality of the response function that was achieved with the combined information on the em shower fraction and the contribution of neutrons to the signals. This Čerenkov signal distribution concerns 200 GeV "jet" events with a Q/S value between 0.70 and 0.75 and a fractional neutron contribution to the scintillator signals between 0.045 and 0.065. The distribution is very well described by a Gaussian fit, with an energy resolution of 4.7%. The resolution was further reduced, to 4.4%, when the neutron fraction was narrowed down to 0.05 - 0.055. As a reminder, we mention that all these results were achieved in a calorimeter with an instrumented mass of only about 1 ton.

3.6 Summary: List of published papers

The experimental results obtained by the DREAM Collaboration, some of which were shown in the previous subsections, are summarized in the following 17 papers:

1. N. Akchurin *et al., Muon Detection with a Dual-Readout Calorimeter*, Nucl. Instr. and Meth. **A533** (2004) 305 – 321.

2. N. Akchurin *et al., Electron Detection with a Dual-Readout Calorimeter*, Nucl. Instr. and Meth. **A536** (2005) 29 – 51.

3. N. Akchurin *et al., Hadron and Jet Detection with a Dual-Readout Calorimeter*, Nucl. Instr. and Meth. **A537** (2005) 537 – 561.

4. N. Akchurin *et al., Comparison of High-Energy Electromagnetic Shower Profiles Measured with Scintillation and Čerenkov Light*, Nucl. Instr. and Meth. **A548** (2005) 336 – 354.

5. N. Akchurin *et al., Separation of Scintillation and Čerenkov Light in an Optical Calorimeter*, Nucl. Instr. and Meth. **A550** (2005) 185 – 200.

6. R. Wigmans, *The DREAM Project – Results and plans*, Nucl. Instr. and Meth. **A572** (2007) 215 – 217.

7. N. Akchurin *et al., Measurement of the Contribution of Neutrons to Hadron Calorimeter Signals*, Nucl. Instr. and Meth. **A581** (2007) 643 – 650.

8. N. Akchurin *et al., Contributions of Čerenkov Light to the Signals from Lead Tungstate Crystals*, Nucl. Instr. and Meth. **A582** (2007) 474 – 483.

9. N. Akchurin *et al., Comparison of High-Energy Hadronic Shower Profiles Measured with Scintillation and Čerenkov Light*, Nucl. Instr. and Meth. **A584** (2008) 273 – 284.

10. N. Akchurin *et al., Dual-Readout Calorimetry with Lead Tungstate Crystals*, Nucl. Instr. and Meth. **A584** (2008) 304 – 318.

11. N. Akchurin *et al., Effects of the Temperature Dependence of the Signals from Lead Tungstate Crystals*, Nucl. Instr. and Meth. **A593** (2008) 530 – 538.

12. N. Akchurin *et al., Separation of Crystal Signals into Scintillation and Čerenkov Components*, Nucl. Instr. and Meth. **A595** (2008) 359 – 374.

13. N. Akchurin *et al., Neutron Signals for Dual-Readout Calorimetry*, Nucl. Instr. and Meth. **A598** (2009) 422 – 431.

14. N. Akchurin *et al., Dual-Readout Calorimetry with Crystal Calorimeters*, Nucl. Instr. and Meth. **A598** (2009) 710 – 721.

15. N. Akchurin *et al., New Crystals for Dual-Readout Calorimetry*, Nucl. Instr. and Meth. **A604** (2009) 512 – 526.

16. N. Akchurin *et al., Dual-Readout Calorimetry with a Full-Size BGO Electromagnetic Section*, Nucl. Instr. and Meth. **A610** (2009) 488 – 501.

17. N. Akchurin *et al., Optimization of Crystals for Applications in Dual-Readout Calorimetry*, submitted to Nucl. Instr. and Meth. (2010).

The author list of these papers also illustrates how the DREAM Collaboration has evolved in the period from 2002 - 2010.

4 Future Research Plans

Based on the results obtained in the past seven years, decribed in the previous sections, we believe to have all the ingredients in hand to build a calorimeter system that will meet and exceed the requirements of experiments at a future linear electron-positron collider, and that will set performance records in all relevant aspects of calorimetry. To verify this statement, we plan to construct two detectors:

1. A *fiber detector*, built according to the principles of the original DREAM calorimeter, but sufficiently large to contain high-energy hadron showers at the 99% level, and including a number of modifications addressing the weak points of the original detector.

2. A *crystal matrix*, sufficiently large to serve as the electromagnetic section of a hybrid system in which the fiber calorimeter backs it up. The readout of this crystal matrix is designed such that em showers can be detected with high resolution, and that the Čerenkov component of the light signals can be extracted with adequate purity and signal strength.

These two calorimeters will be tested individually and in combination in high-energy beams of electrons, hadrons and multi-particle "jets". The construction of the fiber detector has started and we expect to be able to test the first module of this detector this summer in a particle beam. In the following, some crucial aspects of these detectors, and the necessary design modifications of our existing calorimeters, are discussed.

4.1 Detector size

If one wants to improve the performance of an existing calorimeter, one should first and foremost concentrate on the factors that limit that performance. This was the driving principle behind the original DREAM project, and should also be the guiding principle of the new project. The detectors we built so far were too small to fully contain high-energy hadronic showers. Lateral energy leakage was **the** factor dominating the energy resolution after the fluctuations in $f_{\rm em}$ were eliminated.

The importance of lateral shower leakage fluctuations was already evident *before* the dual-readout corrections were applied to the signals, as illustrated by Figure 21. In the measurements in which we tested the BGO crystal matrix in conjunction with the fiber calorimeter, the latter was surrounded by a number of large plastic-scintillator slabs. Some of these are visible in Figure 15. The signals from these scintillators were used as a measure of the lateral shower leakage.

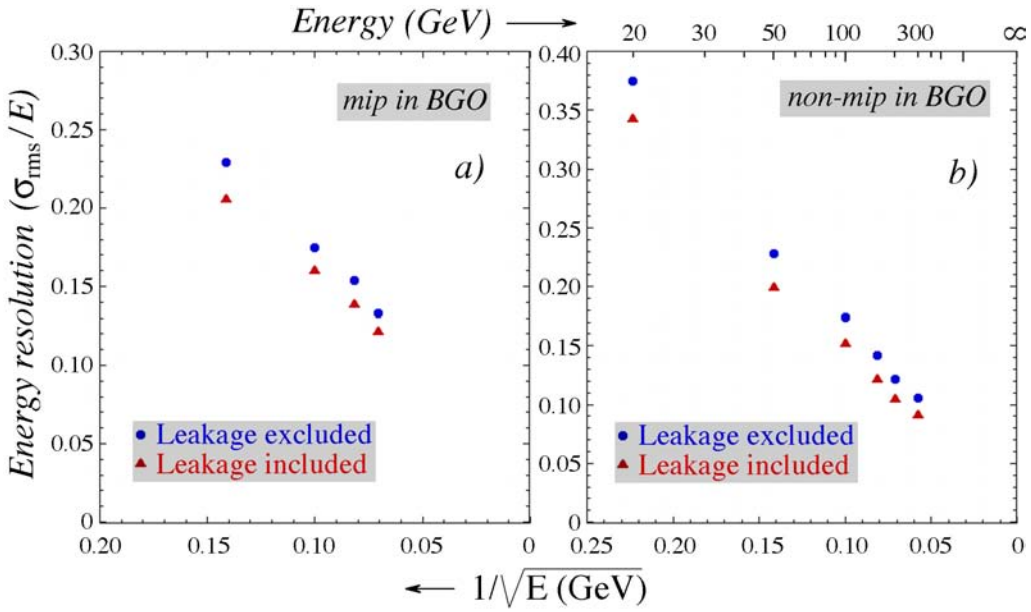

Figure 21: Energy resolution for single pions that penetrated the BGO ECAL without starting a shower, measured with the scintillation signals alone. Results are given with and without taking into account the signals from the leakage counters (a). Energy resolution for single pions that started their shower in the BGO ECAL, measured with the scintillation signals alone. Also here, results are given with and without taking into account the signals from the leakage counters (b) [17].

Figure 21 shows the resolution of the hadronic signals ($\sigma_{\rm rms}$/mean) before and after including the signal contributions from these leakage counters [17]. Despite the extremely crude setup with which the leakage information was obtained, it improved the hadronic energy resolution by 10-15%. This was true both for showers starting in the BGO (Figure 21b) and for particles that penetrated the BGO before starting to shower and deposited all their energy in the fiber calorimeter (Figure 21a), even though the leakage counters only covered the fiber section of the calorimeter system. The data shown in Figure 21 imply that lateral leakage fluctuations alone contributed about 4% to the hadronic energy resolution at 300 GeV, and more at lower energies, in agreement with the $E^{-1/4}$ dependence that is typical for this effect [3].

To put this in perspective, we show in Figure 22a the results of measurements of hadronic shower containment. These data were derived from measurements of the average lateral shower profile, which were performed by sending a beam of 100 GeV pions into a number of different impact points over the surface area of the fiber calorimeter [10]. On average, 90% of the scintillation light that would have been produced in an infinitely large calorimeter of this type was detected when the beam hit the calorimeter in its geometrical center. The improvement observed in Figure 21 was thus the result of the elimination (or rather, reduction) of *fluctuations* in the 10% leakage. At 100 GeV, these fluctuations were measured to contribute $\sim 6\%$ to the total energy resolution.

Figure 22b shows that leakage fluctuations also affect the dual-readout procedure. The relationship between the Čerenkov/scintillator signal ratio, which is measured, and the em shower fraction, which we need to know in order to eliminate the effect of fluctuations in that fraction,

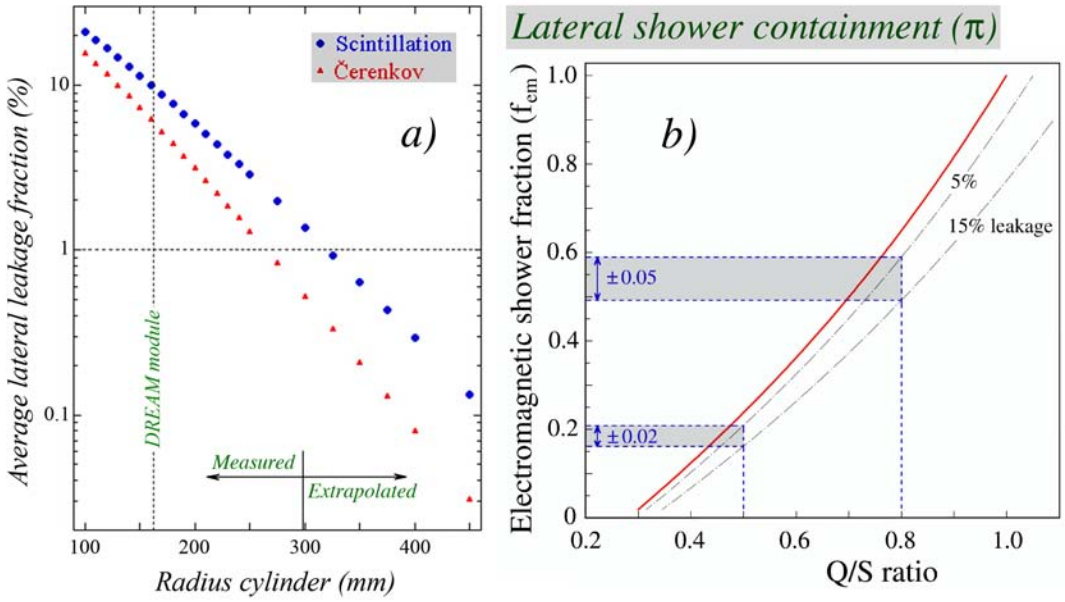

Figure 22: Leakage outside of a DREAM calorimeter cylinder, as a function of the radius of that cylinder. Results are given as a fraction of the total signal in an infinitely large calorimeter, separately for scintillation and Čerenkov light (a). The relationship between the Q/S signal ratio and the em shower fraction, $f_{\rm em}$. Also shown is how a shower leakage of $10 \pm 5\%$ translates into an uncertainty in the em shower fraction (b) [10].

is indicated by the red curve. The dashed curves show how this relationship is changed when the shower leakage amounts to 5% or 15%, respectively. Since the shower leakage typically fluctuates between these two values, an uncertainty is introduced in the $f_{\rm em}$ values derived on the basis of the measured signals.

The profile measurements also show how large the detector has to be made to reduce the average side leakage to a desired level. We believe that this level has to be set at 1%, *i.e.* an average containment of 99%. The contribution of leakage fluctuations to the hadronic energy resolution would then be reduced to $< 1\%$ at the highest energies at which this detector could be tested, and become comparable to or smaller than the contributions of the other effects we try to reduce in the design of this detector.

Figure 22a shows that the effective radius of the fiber calorimeter would have to be ≈ 30 cm to achieve that goal, provided of course that the detector composition would not change. The instrumented mass of the calorimeter would become about 5000 kg. If the granularity was kept the same as in the prototype, the number of readout cells would increase from 19 to 61, and the number of electronic channels from 38 to 122.

4.2 Fibers

Compared to the prototype detector, a number of changes will be made with respect to the fibers. These modifications concern the type of Čerenkov fibers, the fiber diameter, the ratio of the two types of fibers, the packing fraction, and the way the fibers are distributed over the detector volume. The goal of these changes is to reduce the effects of sampling fluctuations

and fluctuations in the number of photoelectrons on the energy resolution to values less than $0.15E^{-1/2}$. An important boundary condition derives from the fact that the detectors that read out the light should fit within the detector perimeter. Because of this condition, the packing fraction of the prototype calorimeter (*i.e.* the fraction of the detector volume occupied by fibers) was $\sim 22\%$. This number will be increased to about 43% in the new, full-scale calorimeter[5].

4.2.1 Light yield considerations

In order to limit the effects of signal quantum fluctuations on the energy resolution to $0.15E^{-1/2}$, the light yield has be larger than 40 photoelectrons per GeV deposited energy. This requirement is especially important for the Čerenkov signal, because of the relatively small probabilities for Čerenkov photon emission. Since the Čerenkov signal is almost entirely limited to the em shower component, which constitutes typically half of the total shower energy, our goal should be a light yield of ~ 80 photoelectrons per GeV for the Čerenkov component. That is a factor of 10 (4.5) more than we measured for the quartz (clear plastic) fibers used in our prototype [20]. The light yield can be increased in the following ways:

1. By using fibers with a larger numerical aperture.
2. By increasing the Čerenkov sampling fraction.
3. By using a light detector with a larger quantum efficiency for Čerenkov light.

Each of these options offers the opportunity to at least double the light yield, so that the required light level is most definitely achievable. The final design is based on an optimal combination of these improvement factors.

4.2.2 Sampling fluctuations

Together with the small Čerenkov light yield and the effects of side leakage, sampling fluctuations limited the stochastic term in the energy resolution of the DREAM fiber calorimeter to $\sim 0.6E^{-1/2}$ (Figure 9b). Sampling fluctuations usually dominate the resolution of electromagnetic sampling calorimeters. It has been demonstrated that they are determined both by the sampling *fraction* and the sampling *frequency*, and are well described by [3]

$$\frac{\sigma_{\rm samp}}{E} = \frac{a}{\sqrt{E}}, \qquad \text{with } a = 0.027\sqrt{d/f_{\rm samp}} \tag{5}$$

where d denotes the thickness of the individual sampling layers (in mm) and $f_{\rm samp}$ the sampling fraction for mips (Figure 23). The sampling fluctuations for hadrons are typically twice as large as those for em showers in the same sampling calorimeter. It is important to realize that, for the purpose of sampling fluctuations, a calorimeter of this type consists actually of two completely independent sampling structures, and that the sampling fluctuations in one structure (*e.g.* copper/scintillator) are not at all affected by those in the other structure (Čerenkov/copper).

[5]For reference purposes, we mention that the packing fraction in the KLOE detector [19], which set the record in this respect, was 48%.

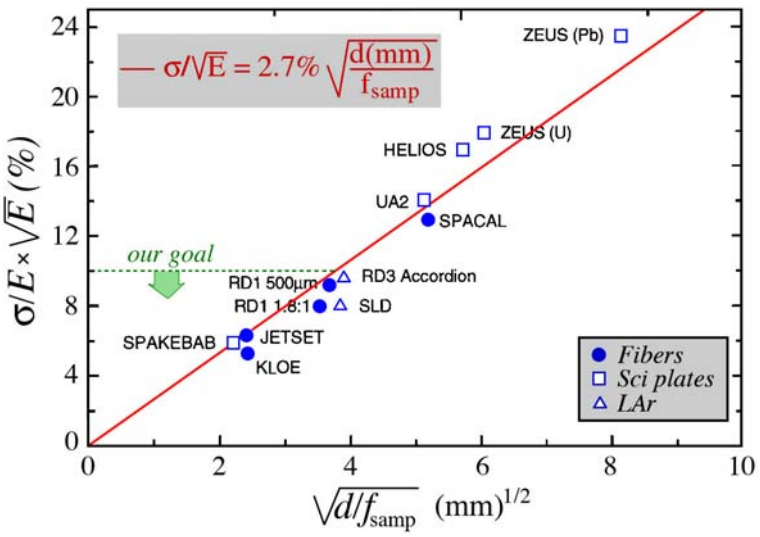

Figure 23: The em energy resolution of sampling calorimeters as a function of the parameter $(d/f_{\rm samp})^{1/2}$, in which d is the thickness of an active sampling layer (*e.g.* the diameter of a fiber or the thickness of a liquidargon gap), and $f_{\rm samp}$ the sampling fraction for mips [21].

For the original DREAM fiber calorimeter, the effective thickness of one (scintillation) sampling layer was 1.4 mm, and the sampling fraction was 2.1% for the scintillator/copper structure. According to Equation 5, sampling fluctuations for em showers in this structure should thus scale as $0.218E^{-1/2}$, in good agreement with the experimental result [20]. Options to reduce the sampling fluctuations include:

1. Embedding the fibers individually in the copper structure, and not in groups of seven (see Figure 5). This increases the sampling frequency.

2. Reducing the fiber diameter. This also increases the sampling frequency.

3. Increasing the sampling fraction by increasing the overall fiber filling fraction.

We have chosen to use the first and last of these options in our new detector. Especially the change to a "KLOE-type" geometry, in which fibers are embedded individually, rather than in bunches, will lead to a substantial improvement. By combining the signals from the two types of fibers, we expect to reduce the contribution of sampling fluctuations to the em energy resolution to $0.077E^{-1/2}$, and to twice as much for the hadronic energy resolution.

In this context, we want to point out that sampling fluctuations were also the dominating factor that limited the hadronic energy resolution of compensating calorimeters such as SPACAL and ZEUS to $0.3 - 0.35E^{-1/2}$. Reducing the (effects of) sampling fluctuations is going to be the area where potentially most of the improvement of these (record setting) results can be achieved. This is made possible by the fact that, unlike in the other mentioned detectors, dual-readout calorimeters are not bound to a specific (small) sampling fraction. We exploit this advantage to the fullest extent that is practically possible.

4.3 Light detectors

In recent years, a number of interesting developments in the area of light detection have taken place. Silicon photomultipliers, avalanche photo diodes and hybrid photon detectors each offer interesting features and promise for the future. However, for the essential aspects that are important for dual-readout calorimetry, we believe that at this point in time PMTs are the best choice, at least for the fiber calorimeter. Listed below are the essential properties of the light detectors for the fiber calorimeter.

1. A sufficiently large photocathode surface. The fibers alone cover already about half of the exit surface of the calorimeter.

2. Very low noise. The shower signals are shared among more than 100 channels, most of which see less than 0.1% of the light. Yet, including these peripheral towers is crucial for obtaining the excellent energy resolution envisaged. We know this first-hand from our experience with SPACAL (Figure 24).

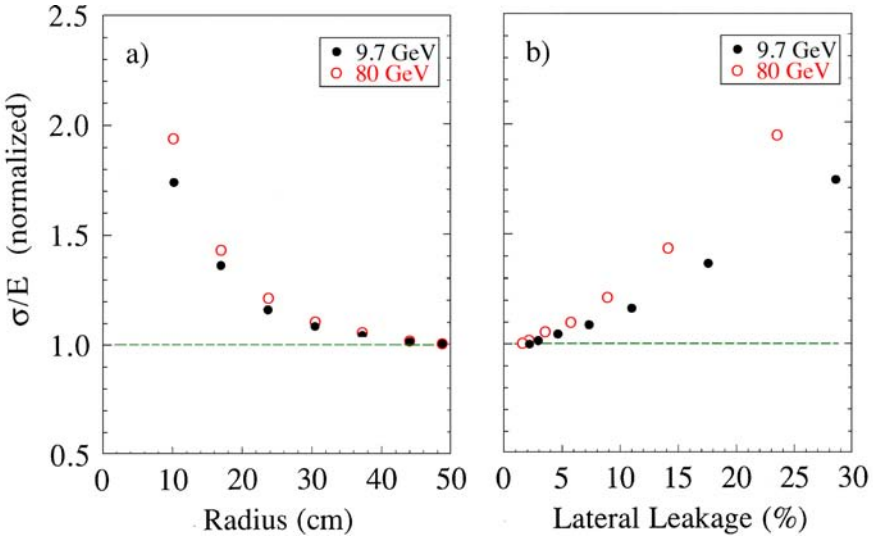

Figure 24: The hadronic energy resolution as a function of the effective radius of the area over which the SPACAL signals were integrated (a), and as a function of the average lateral shower leakage (b). Data for 9.7 and 80 GeV pion showers. The energy resolutions have been normalized to the values obtained for complete shower containment [22].

3. A large dynamic range. The signals may consist of singe photoelectrons (in the shower tails) or tens of thousands of photoelectrons (in the em core of energetic hadron showers).

4. A large quantum efficiency. This is especially important for the detectors of the Čerenkov light, since it directly affects the energy resolution of the dual-readout calorimeter.

5. A large ratio between the effective photocathode surface area and the outside perimeter of the tube. This maximizes the possible fiber packing fraction. This criterion favors square, compact PMTs.

6. The signals should be sufficiently fast to recognize and accurately measure the amplitude of the 20 ns tail caused by the neutron contributions.

The requirements are somewhat different for the crystals, and therefore the choice of the light detector may be different as well. Regardless of the type of crystal chosen for the electromagnetic calorimeter section, two criteria are of great importance.

1. Compactness. The distance between the em and hadronic calorimeter sections must be as small as possible, ideally not more than a few cm.

2. Insensitivity to charged particles. When traversed by charged particles, some light detectors, in particular silicon-based photodiodes, produce a signal that is equivalent to that from thousands (and in some cases millions) of photons. Such detectors are completely unsuited for our purpose, since the area between the two calorimeter sections will typically be traversed by a large number of shower particles, especially when em showers have started $\sim 5 - 10X_0$ before this gap. Densely ionizing particles produced in nuclear reactions, which may have specific ionizations 3 orders of magnitudes larger than mips may generate huge signals in such detectors, as recently experienced by CMS.

In addition, the light detectors should be sufficiently fast to isolate the prompt Čerenkov component in the crystal signals from the slower scintillation component. This criterion depends of course on the specifics of the chosen crystal, as may be illustrated by a comparison between Figures 12 and 14. Also, they should cover a sufficiently large fraction of the crystal surface to guarantee the necessary yield of Čerenkov photoelectrons.

4.4 Crystals

In the tests described in Section 3, we have investigated the properties of two readily available crystals for dual-readout purposes: Lead tungstate ($PbWO_4$) and bismuth germanate ($Bi_4Ge_3O_{12}$, or BGO). Even though the relative Čerenkov component in the light produced by $PbWO_4$ is considerably larger than for BGO, the latter crystal was much better suited for dual-readout calorimeter purposes because of the difference in the characteristic optical spectra, and the long decay time of the scintillation component, although the latter is too long for applications in many particle physics experiments.

New crystals that have been specifically developed for dual-readout calorimetry are based on lead tungstate, and doped with a substance that shifts the scintillation spectrum to longer wavelengths and increases the decay time. The first tests of such crystals were already quite successful (Figure 3). In a crystal doped with 1% molybdenum, almost completely pure Čerenkov and scintillation spectra were obtained with different optical transmission filters, and the decay time of the scintillation process had increased to the very useful value of 26 ns. The only disadvantage of this crystal was the strong attenuation of the Čerenkov light, which also suppressed the Čerenkov light yield [6]. In the next iteration, crystals with smaller fractions of molybdenum were tested, in conjunction with a variety of filters intended to select the Čerenkov component of the signals. The light attenuation was clearly less and the Čerenkov light yield considerably higher in this case [18].

Yet, light attenuation is a concern and so is the production of Čerenkov light in the light detector itself (filter, window). For this reason, we envisage a crystal matrix that is read out from two sides (upstream and downstream). Downstream, the light will be filtered so that *only* Čerenkov light is transmitted. Upstream, a mixture of scintillation and Čerenkov light is detected. The upstream signal, dominated by the isotropically emitted scintillation light, will be used to measure the energy of photons and electrons showering in the detector. By comparing the intensity of the upstream and downstream Čerenkov signals, effects of light attenuation and the contribution of charged shower particles to the downstream signals can be recognized and eliminated. We intend to test these procedures this summer in our next round of beam tests, using a small matrix of $PbWO_4$:0.3%Mo crystals specially made for this purpose.

4.5 Readout

Probably the most important thing we have learned from all the tests we have performed in the past seven years is the immense value of high-resolution time structure measurements of the calorimeter signals. Such measurements have been absolutely instrumental in separating the Čerenkov and scintillation components of the calorimeter signals (Figures 12 - 14) and in recognizing and measuring the contribution of neutrons (Figure 4).

Until now, our measurements of the time structure of the calorimeter signals have been performed with a digital sampling oscilloscope. This allowed us to obtain this information for a maximum of four electronic channels. In that scheme, measurements of the neutron contribution to the signals were only possible by grouping the signals from many different towers together into one electronic channel, representing, for example, the total Čerenkov signal produced by the fiber calorimeter. In the proposed calorimeters, we want to measure the time structure of *all* signals produced by the individual towers. This will require a cost effective alternative to the $40K oscilloscope.

One candidate solution, which is currently being tested in the context of the DREAM project, is based on the Domino Ring Sampler (DRS) chip, developed at PSI for the MEG experiment [23]. In the present version IV of this chip, the sampling frequency is set to 2 GHz, with an intrinsic bandwidth of about 400 MHz. Each chip can host up to 10 analog channels, for a power consumption of 35 mW. The sampler is made of two sections, an analog section for the signal sampling and a digital section for control and multiplexing. In the analog section, an array of 1024 switching capacitors samples the input signal at the frequency determined by the Domino Wave. Once a trigger is received, the capacitors are sequentially readout by a pipeline 12-bits ADC, starting from the trigger leading edge moving backward. In this way, the time history of the signal is stored in the output, while the trigger signal itself is stored in a DRS channel. The CAEN company has become interested in this project and will soon release a commercial version. An 80-channel readout system based on an earlier version of this chip (DRS-II), derived from the MAGIC DAQ system, was tested in the context of the DREAM project in 2008. We were able to reproduce the neutron fraction measurements shown in Figures 4 and 18. In 2009, BGO pulse shapes (Figure 14) were successfully reproduced with the DRS-IV chip.

One other major modification of the readout system used for the existing prototype will concern the front-end signal digitization. For historical reasons, related to the (lack of) accessibility

of the detectors during our beam tests, all analog signals were transported to the counting room, using 45 m (!) long cables. Despite the fact that special low-loss cables were selected for this purpose, the effects on the time structure of the signals were not negligible. Apart from that, treating a few hundred signals that way is not very practical. For these reasons, we intend to redesign the front-end electronics from scratch. All signal digitization will take place as close to the place where these signals are generated as possible.

4.6 The new DREAM detectors

Even though some details of the new detectors remain open for improvement, in the spirit of the considerations presented in the previous subsections, we have started the construction. Initially, we will concentrate most of our efforts on the fiber calorimeter. The crystal em section will be completed at a later date, based on

- The results of tests with individual crystals and small matrices, which are intended to lead to an optimal design of the em section
- The availability of funding. At this moment, only funding for the fiber calorimeter has been secured.

Most of the construction efforts are currently concentrated in Italy.

4.6.1 The fiber calorimeter

The structure of the proposed fiber calorimeter is inspired by the SPACAL [22] and KLOE [19] calorimeters built previously. Figure 25a shows the pattern according to which the two types of fibers will be distributed over the detector volume. The construction of this structure will be based on the techniques developed by the KLOE Collaboration. Alternating layers of scintillating and Čerenkov fibers will be glued onto the two sides of thin grooved copper foils, displaced by half a pitch. The copper foils have passed through special rollers such as to produce the desired shape. The copper foils are 1.0 mm thick, both types of fibers have a diameter of

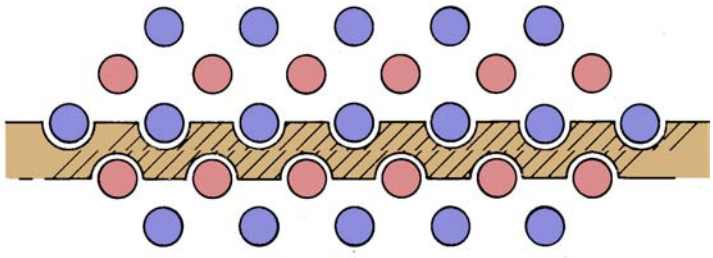

Figure 25: The pattern according to which the two types of fibers will be distributed inside the detector volume (not to scale).

1.0 mm and are spaced by 1.35 mm (center-to-center). The resulting structure has an effective nuclear interaction length of ~ 25 cm, an effective radiation length of ~ 2.8 cm and an effective

Figure 26: The machine with which the 1 mm thick copper foils are being rolled into the desired shape, and the result of this process.

Moliére radius ~ 2.6 cm Figure 26 shows the machine with which the copper foils are being rolled and the resulting shape of these foils.

The detector will consist of modules, which contain 4 towers each. Each module is read out by means of 8 PMTs, 4 for each type of fiber. Each module has a square cross section of 90×90 mm^2 , is 2.5 m (10 $\lambda_{\rm int}$ long, contains 4224 fibers (2112 of each type) and weighs ~ 170 kg.

The calorimeter will be readout by means of square fine-mesh PMTs. This choice would minimize the transverse area occupied by these light detectors, since no magnetic shielding will be needed. Hamamatsu R-8600-03 tubes are well suited for this purpose. Their outside dimensions are 2.54×2.54 cm^2, while the photocathode area measures 2.35×2.35 cm^2 (*i.e.* $> 85\%$ of the outer envelope!). This is schematically shown in Figure 27.

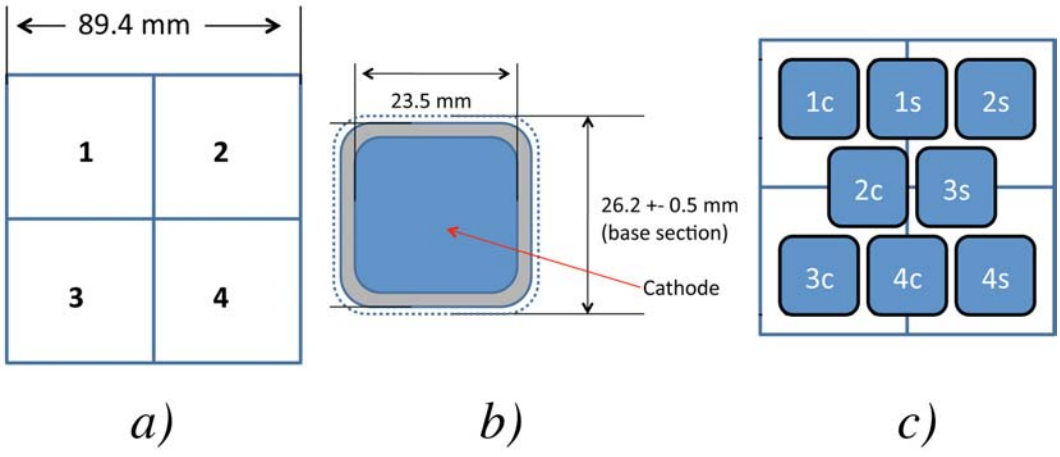

Figure 27: Each module consist of 4 square towers (a), which are read out by means of square PMTs (b), which are mounted at the rear as shown in c.

Equipped with a super-bialkali photocathode, the quantum efficiency of these tubes would be more than a factor of two larger than for the PMTs used in our fiber prototype. Combined with the increased numerical aperture of the chosen clear plastic fibers (0.72 *vs.* 0.33 for the quartz fibers and 0.50 for the plastic fibers used in the original prototype) and the increased sampling

fraction (a factor 2), we expect the Čerenkov light yield to be more than adequate.

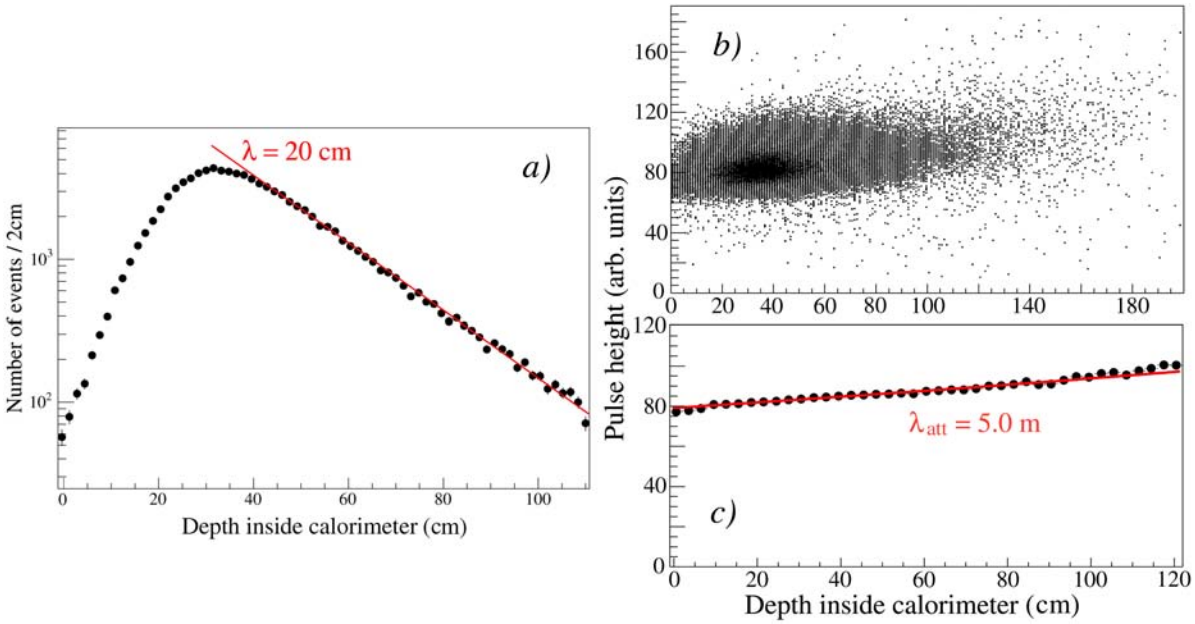

Figure 28: Distribution of the average depth at which the scintillation light is produced in the DREAM calorimeter by showering hadrons (a). Scatter plot showing the total scintillator signal versus the average depth of the light production (b) and the average size of the total scintillator signal as a function of that depth (c), for events induced by 100 GeV π^- mesons [5].

We will have the option to time-sample every signal at a rate of up to 5 GHz. Apart from the need to measure the contribution of neutrons to the scintillator signals, this time sampling may turn out to be very important for providing depth information on the signals from this longitudinally unsegmented detector. Knowledge of the depth at which the light production is concentrated is important for eliminating the effects of light attenuation, which is a problem in the scintillating fibers, especially if one aims for high resolution. We have measured typical light attenuation lengths of 5 m in the scintillating fibers used in the DREAM calorimeter. Shower fluctuations on a scale of one nuclear interaction length (25 cm) thus lead to an energy-independent term in the energy resolution of 25/500 $\sim 5\%$, if one does not know at which depth the light was produced in the events.

As illustrated in Figure 28, this effect was clearly observed in beam tests of the DREAM fiber calorimeter. The deeper inside the calorimeter the light production took place, the larger the response. In these tests, the depth of the light production was determined by comparing the impact point of the beam particle with the (lateral) center-of-gravity of the light production in the various calorimeter towers. The calorimeter was oriented at a small angle (3°) with respect to the beam line to make this procedure possible.

The detailed time structure of the signals may make it possible to obtain this information also for particles that enter the detector exactly along the fiber direction. It may also make it possible to determine the shower depth for neutral particles and jets, for which the above procedure does not work.

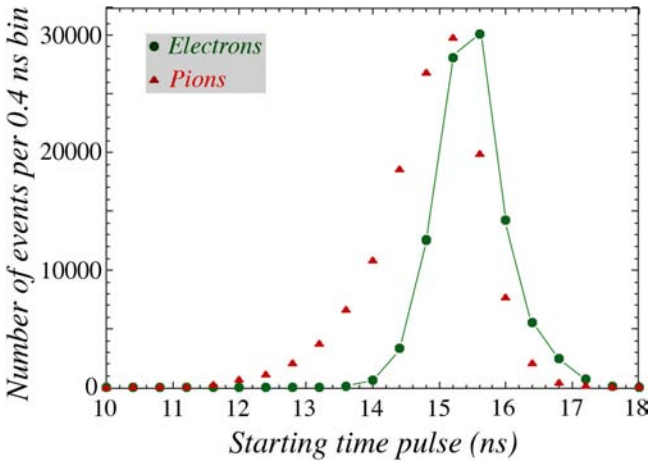

Figure 29: Starting point of the signals generated by electrons and pions in the original DREAM fiber calorimeter. The time was measured with respect to the passage of the beam particle through an upstream trigger counter.

Light typically travels at a speed (c/n) of 17 cm per nanosecond in these fibers, whereas the shower particles that generate the light travel at c (30 cm/ns). Therefore, the deeper inside the calorimeter the light is produced, the earlier the photons reach the photocathode. This effect is illustrated in Figure 29, which shows the distribution of the starting time of the PMT signals for electron and pion showers developing in the original fiber calorimeter. The figure shows that the light generated by the pion showers arrived earlier and had a larger event-to-event spread than the light generated by the electron showers. These results were obtained with PMTs that had considerably larger rise and transit times than the PMTs we will use for the new detector, and we expect to be able to measure the depth of the light production with substantially better precision. Measurement of this precision is one of our goals in the experimental program for this summer.

4.6.2 The crystal matrix

As pointed out earlier, construction of the crystal matrix is at this point clearly a lower priority for us. More data (and money) will be needed before we can proceed with this. Our current ideas about this matrix are described below.

The transverse size of the crystal matrix will be somewhat smaller than that of the fiber calorimeter, since this matrix will only see the early, more collimated part of the showers. The effective radius will be 20 cm instead of 30 cm. In total 140 crystals with transverse dimensions of 3×3 cm^2 will be needed for that. The current best candidate crystal is $PbWO_4$, doped with a fraction of 1% molybdenum. The crystals will be 20 cm deep (22.5 X_0). Each crystal will be readout from both sides with a suitable PMT. The Hamamatsu R-8600U, equipped with an ultra-bialkali photocathode and a UV-transparent window, is also a good candidate for this purpose. Its effective photocathode area of 23.5×23.5 mm^2 will cover more than 61% of the crystal surface. On the downstream side, UV transmission filters will be mounted between the crystals and the PMT, on the upstream side blue transmission filters. All signals will be time sampled at a rate of 2 GHz. Figure 30 shows how the average time structure of the signals produced by high-energy electron showers in this crystal changes as a function of the cut-off wavelength

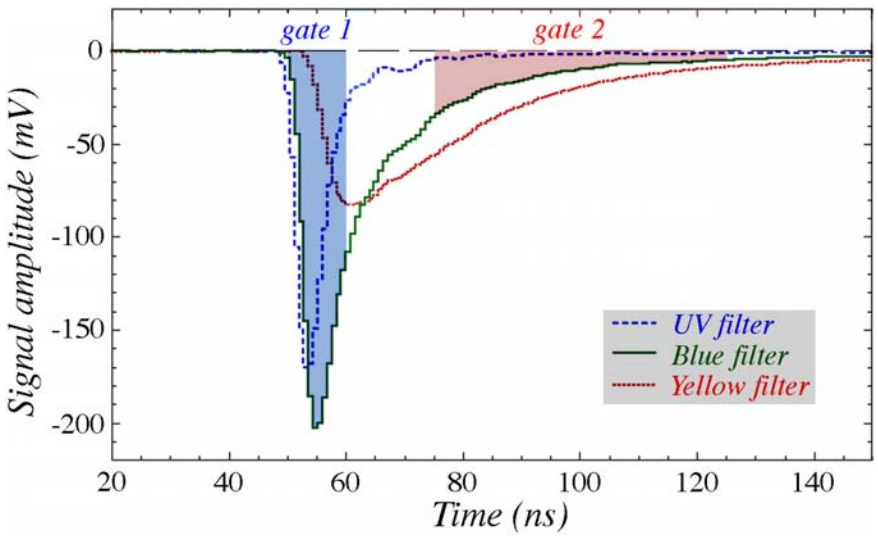

Figure 30: Average structure of the signals from a $PbWO_4$ crystal doped with 1% of molybdenum. The light generated in this crystal by 50 GeV electrons was transmitted either through a UV, a blue or a yellow filter [6].

of the light transmitted through different optical filters. The UV filter transmits only Čerenkov light, and the light transmitted by the yellow filter is strongly dominated by scintillation. The blue light consists of a mixture of both types. With gates over the early and late parts of the time structure, the signal can be unraveled event by event into these two components, in the same way as described for BGO (Figure 14).

All front-end electronics will be mounted on the detector. This front-end electronics could include a processor that derives the Čerenkov/scintillation ratio of the crystal signals from the time structure of the signals. Only digitized information will be sent to the counting room.

5 Support requested from CERN

In the past 7 years, the beam tests of the DREAM Collaboration have been carried out in the H4 beam (location H4A) of the SPS. Typically, we were allocated 10 - 14 days per year for this purpose. Over the years, it has become gradually more and more difficult to obtain the data (and the data quality) needed for our work, because of the following reasons:

- The fact that the H4A area, as well as the associated counting room, had to be shared by an increasing number of different user groups
- The increased complexity of the tests we wanted to do (more readout channels)
- The reduced accessibility of the H4A area, as a result of the low-energy modifications of the neighboring H2 beam
- The increased distance to the counting room (cable length 45 m!) as a result of these modifications

Since we had to set up, test our cables and connections every year from scratch, precious beam time was lost, and mistakes were inevitable. The time structure of the signals, which is crucial for much of what we do, had to be measured at the end of increasingly long cables, which inevitably introduced distortions. Now that we are moving into a new, conclusive phase of this project, we would like to start our test beam setup from scratch in a new location, with the following characteristics:

- The possibility to make a permanent experimental setup, which can be moved out of the beam if and when needed without disconnecting the readout
- The possibility to run with low-energy beams of pions and (less important) electrons
- Easy access, except of course during downstream beam tests
- Close proximity of a counting room dedicated to this experiment, where electronics and DAQ can be installed on a permanent basis

In this context, permanent means of course for the duration of this project, which we currently estimate at 3-4 years. We have discussed this issue with the people responsible for operations in the North Area, in particular with Dr. Ilias Efthymiopoulos, and identified a suitable solution in the H8 beam, just upstream of the TOTEM test setup.

We would like to ask the SPSC to approve our request to adapt this area for our experimental beam test program, for the period 2010 - 2013. This would most notably involve installation of a suitable moveable support table (maximum weight 10 tons, moveable in x, y and if possible θ). In addition, some cable trays would be needed. We also like to request that the low-energy (tertiary target) option be made available again in H8. Other groups, especially ATLAS, have used this beam line in the past to test their detectors with particles down to 2 GeV/c. Such tests are very important for hadron calorimeters, since a large fraction of high-energy jets is carried by particles with energies below 10 GeV. Such beams were unfortunately not available in H4A.

As part of this request, we would also like to ask for some technical support. Projects of this type often require the intervention of technicians, to deal with unforeseen problems of one type or another. We are planning to bring our own technicians to CERN, but they might need access to specific workshop equipment. Occasional assistance from the CERN technicians associated with the North Experimental Area would also be appreciated.

6 Concluding remarks

The developments in observational sciences such as biology, astronomy and physics have always been driven by the quality of the tools with which the observations are being made. The development of the microscope, the telescope and ever more powerful particle accelerators have led to quantum leaps in our understanding of the functioning of living organisms, the notion of our place in space and time and the innermost structure of matter.

Sometimes, factors unrelated to the quality of our instruments prevent further improvement. For example, the angular resolution of a telescope is ultimately limited by diffraction (Rayleigh's

criterion). However, in practice atmospheric turbulence limits this resolution to values that are much larger than the diffraction limit. In such situations, ingenuity is needed: Using optical interferometry between different telescopes, the effects of this turbulence can be measured and thus greatly reduced.

In the last quarter century, calorimeters have evolved as the particle detectors of choice in experiments at the energy frontier. However, development of the full potential of these detectors is hampered by an effect comparable to the atmospheric turbulence mentioned above. In this case, the problem is caused by the fact that electrons and photons generated in the absorption process produce significantly larger signals than equally energetic protons and pions generated in this process. The fact that the energy sharing between these different classes of shower particles (the electromagnetic fraction, $f_{\rm em}$) varies strongly and in a non-Gaussian manner from one event to the next and is, on average, energy dependent, creates a whole series of awkward problems (non-linearity, non-Gaussian response functions, *etc.*) that could be avoided in the absence of this effect.

High-quality energy measurements will be an important tool for accelerator-based experiments at the TeV scale. There are no fundamental reasons why the four-vectors of all elementary particles could not be measured with a precision of 1% or better at these energies. However, reaching this goal is far from trivial, especially for the hadronic constituents of matter. Unfortunately, little or no guidance is provided by hadronic Monte Carlo shower simulations in this respect. In the past 30 years, all progress in this domain therefore has been achieved through dedicated R&D projects, and this is still the way to go today.

Several major R&D efforts are underway to further improve the quality of hadronic energy measurements. These efforts are characterized by very different styles. R&D in the framework of the Particle Flow Analysis concept is to a large extent concentrated on the technicalities of detector design, whereas very fundamental questions concerning crucial aspects of the applicability of this concept (*e.g.* calibration, experimental tests of PFA algorithms) tend to be ignored. On the other hand, the purely generic dual-readout R&D project concentrates strongly on experimental tests of the validity of the principles on which improvement of the hadronic calorimeter performance is based, and tends to ignore issues concerning the incorporation of this type of detector into a 4π experiment, and simulations in general [24].

Until now, the dual-readout approach has been remarkably successful. We have established that the dual-readout approach combines the advantages of compensating calorimetry with a reasonable amount of design flexibility. It holds the promise of high-quality calorimetry for *all* types of particles, with an instrument that can be calibrated with electrons.

The DREAM project meets with considerable interest, both inside the high-energy physics community and outside. We have received numerous invitations to speak at departmental colloquia and at international conferences about this project. At the CALOR04 Conference, where DREAM results were presented for the first time, the summary speaker called dual-readout the most important breakthrough innovation in calorimetry in the last decade.

We hope and trust that the CERN SPSC will approve the described continuation of our research efforts and support the requested use of CERN facilities for this purpose.

References

[1] R. Wigmans, *Quartz Fibers and the Prospects for Hadron Calorimetry at the 1% Resolution Level*, Proc. of the VIIth Int. Conf. on Calorimetry in High Energy Physics, Tucson 1997 (World Scientific, Singapore, 1998), p. 182 - 193.

[2] R. Wigmans, *Energy Measurements at the TeV Scale*, New Journal of Physics **10** (2008) 025003.

[3] R. Wigmans, *Calorimetry - Energy Measurement in Particle Physics*, International Series of Monographs on Physics, vol. 107, Oxford University Press (2000).

[4] N. Akchurin *et al.,* Nucl. Instr. and Meth. **A399** (1997) 202.

[5] N. Akchurin *et al.,* Nucl. Instr. and Meth. **A537** (2005) 537.

[6] N. Akchurin *et al.,* Nucl. Instr. and Meth. **A604** (2009) 512.

[7] G. Drews *et al.,* Nucl. Instr. and Meth. **A290** (1990) 335.

[8] N. Akchurin *et al.,* Nucl. Instr. and Meth. **A581** (2007) 643.

[9] N. Akchurin *et al.,* Nucl. Instr. and Meth. **A598** (2009) 422.

[10] N. Akchurin *et al.,* Nucl. Instr. and Meth. **A584** (2008) 273.

[11] N. Akchurin *et al.,* Nucl. Instr. and Meth. **A548** (2005) 336.

[12] N. Akchurin *et al.,* Nucl. Instr. and Meth. **A533** (2004) 305.

[13] N. Akchurin *et al.,* Nucl. Instr. and Meth. **A550** (2005) 185.

[14] N. Akchurin *et al.,* Nucl. Instr. and Meth. **A582** (2007) 474.

[15] N. Akchurin *et al.,* Nucl. Instr. and Meth. **A595** (2008) 359.

[16] N. Akchurin *et al.,* Nucl. Instr. and Meth. **A593** (2008) 530.

[17] N. Akchurin *et al.,* Nucl. Instr. and Meth. **A610** (2009) 488.

[18] N. Akchurin *et al.,* (DREAM Collaboration), *Optimization of Crystals for Applications in Dual-Readout Calorimetry*, submitted to Nucl. Instr. and Meth..

[19] A. Antonelli *et al.,* Nucl. Instr. and Meth. **A354** (1995) 352.

[20] N. Akchurin *et al.,* Nucl. Instr. and Meth. **A536** (2005) 29.

[21] M. Livan, V. Vercesi and R. Wigmans, *Scintillating-fibre Calorimetry*, CERN Yellow Report 95-02, CERN, Genève, Switzerland (1995).

[22] D. Acosta *et al.,* Nucl. Instr. and Meth. **A308** (1991) 481.

[23] S. Ritt, Nucl. Instr. and Meth. **A518** (2004) 407.

[24] See, however, the work performed for the Letter of Intent of the 4th ILC Collaboration http://www.linearcollider.org/physics-detectors/Detectors